Description of the NASA GEOS Composition Forecast Modeling System GEOS-CF v1.0

Christoph A. Keller[1], K. Emma Knowland[1,2], Bryan N. Duncan[1], Junhua Liu[1,2], Daniel C. Anderson[1,2], Sampa Das[1,2], Robert A. Lucchesi[1,3], Elizabeth W. Lundgren[4], Julie M. Nicely[1,5], Eric Nielsen[1,3], Lesley E. Ott[1], Emily Saunders[1,3], Sarah A. Strode[1,2], Pamela A. Wales[1,2], Daniel J. Jacob[4], Steven Pawson[1]

[1]NASA Goddard Space Flight Center, Greenbelt, MD, USA

[2]Universities Space Research Association, Columbia, MD, USA

[3]Science Systems and Applications, Inc., Lanham, MD, USA

[4]School of Engineering and Applied Sciences, Harvard University, Cambridge, MA, USA

[5]Science Systems and Applications, Inc., Lanham, MD, USA

Corresponding author: Christoph Keller (christoph.a.keller@nasa.gov)

Key Points:

- GEOS-CF is a new modeling system that produces global forecasts of atmospheric composition at 25km^2 horizontal resolution.
- GEOS-CF model output is freely available and offers a new tool for academic researchers, air quality managers, and the public.

Abstract

The Goddard Earth Observing System composition forecast (GEOS-CF) system is a high-resolution (0.25 degree) global constituent prediction system from NASA's Global Modeling and Assimilation Office (GMAO). GEOS-CF offers a new tool for atmospheric chemistry research, with the goal to supplement NASA's broad range of space-based and in-situ observations and to support flight campaign planning, support of satellite observations, and air quality research. GEOS-CF expands on the GEOS weather and aerosol modeling system by introducing the GEOS-Chem chemistry module to provide analyses and 5-day forecasts of atmospheric constituents including ozone (O_3), carbon monoxide (CO), nitrogen dioxide (NO_2), and fine particulate matter (PM2.5). The chemistry module integrated in GEOS-CF is identical to the offline GEOS-Chem model and readily benefits from the innovations provided by the GEOS-Chem community.

Evaluation of GEOS-CF against satellite, ozonesonde and surface observations show realistic simulated concentrations of O_3, NO_2, and CO, with normalized mean biases of -0.1 to -0.3, normalized root mean square errors (NRMSE) between 0.1-0.4, and correlations between 0.3-0.8. Comparisons against surface observations highlight the successful representation of air pollutants under a variety of meteorological conditions, yet also highlight current limitations, such as an overprediction of summertime ozone over the Southeast United States. GEOS-CF v1.0 generally overestimates aerosols by 20-50% due to known issues in GEOS-Chem v12.0.1 that have been addressed in later versions.

The 5-day hourly forecasts have skill scores comparable to the analysis. Model skills can be improved significantly by applying a bias-correction to the surface model output using a machine-learning approach.

Plain Language Summary

Accurate forecasting of the compostion of the atmosphere is important for a variety of applications, including air pollution mitigation, support of satellite and other remote-sensing observations, and research applications. Producing such forecasts is computationally expensive due to the complexity of atmospheric chemistry, which interacts with weather on all scales. Here we present the NASA Goddard Earth Observing System composition forecast (GEOS-CF) system, which produces global forecasts of major atmospheric constituents such as ozone (O_3), nitrogen dioxide (NO_2), and fine particulate matter (PM2.5). On a daily basis, the model tracks the atmospheric concentrations of more than 250 chemical species in more than 55 million model grid cells, computing the interactions between those species using the state-of-the-science GEOS-Chem chemistry model.

We present and in-depth evaluation of the GEOS-CF model through comparison against independent observations. We show how the model captures many observed features of atmospheric composition, such as spatio-temporal variations in air pollution due to changes in pollutant emissions, weather, and chemistry. We also highlight some of the model deficiencies, e.g., with respect to the simulation of aerosol particles. Finally, we demonstrate how surface observations and model data can be combined using machine learning to provide improved local air quality forecasts.

1 Introduction

Near real-time information of global atmospheric composition is invaluable for a wide range of applications, including academic research, airborne and satellite mission support, air

quality forecasting, disaster management, and ecosystem monitoring. However, the numerical simulation of atmospheric chemistry is computationally expensive because it involves hundreds of species that interact with each other on time scales from milliseconds to years, and the species are also influenced by dynamics across a wide range of spatiotemporal scales. This precludes the inclusion of detailed aerosol and reactive trace gases in standard operational numerical weather prediction (NWP) systems. Instead, real-time simulation of atmospheric composition is typically done within a simplified system in order to reduce the computational burden, e.g., by running the model at reduced horizontal resolution or over a regional domain only, using a simplified representation of atmospheric composition, or by coupling a weather model with an offline chemical transport model (CTM) (e.g., Bhattacharjee et al., 2018; Emmons et al., 2020; Flemming et al., 2015; Marécal et al., 2015).

Here we present the NASA Goddard Earth Observing System (GEOS) composition forecast modeling system, GEOS-CF v1.0, which provides global analyses and forecasts of atmospheric composition such as ozone (O_3), carbon monoxide (CO), nitrogen dioxide (NO_2), and fine particulate matter ($PM_{2.5}$) in near real-time at a horizontal resolution of approximately 25x25 km^2. To our knowledge, GEOS-CF is one of only a few global forecasting systems of atmospheric composition conducted in near real-time. The European Centre for Medium-Range Weather Forecasts (ECMWF) offers 5-day global forecasts of aerosols and trace gases at approximately 40x40 km^2 horizontal resolution through the Copernicus Atmosphere Monitoring Service (CAMS, https://atmosphere.copernicus.eu/global-forecast-plots). The US National Center for Atmospheric Research (NCAR) conducts 10-day global forecasts at approximately 100x100 km^2 horizontal resolution based on offline simulations of the Model for Ozone and Related chemical Tracers (MOZART) Chemistry Mechanism in the Community Earth System Model Version 2 (CESM2) (Emmons et al., 2020) driven by GEOS meteorological forecasts (https://www2.acom.ucar.edu/acresp/forecasts-and-near-real-time-nrt-products). Finally, the Finnish Meteorological Institute provides daily 4-day global forecasts of atmospheric composition at approximately 35x35 km^2 resolution using the System for Integrated modeLling of Atmospheric coMposition (SILAM v5.7, http://silam.fmi.fi/). The atmospheric composition forecasts from these models can vary considerably due to differences in the underlying meteorological fields, observational constraints, chemical mechanisms, or assumptions about pollutant emissions. The uncertainties associated with these processes can be difficult to quantify from a single model simulation alone, and the availability of multiple, independently developed models offers great potential to provide better air quality information through combination of a suite of models (Marécal et al., 2015). GEOS-CF offers such an independent composition forecast, thus complementing the existing suite of global composition forecasting systems by providing global 5-day forecasts of atmospheric composition using the GEOS-Chem atmospheric chemistry module (http://www.geos-chem.org) within GEOS from January 2018 onward.

One of the key aspects of the GEOS-CF system is the full integration of the GEOS-Chem model in the GEOS system, which allows for the simulation of reactive gases and aerosols at the same temporal and spatial resolution as the meteorology (Long et al., 2015; Hu et al., 2018). GEOS-Chem is actively evaluated and developed by a large international research community, and the GEOS-Chem module incorporated in GEOS-CF uses the exact same codebase as the offline CTM. This enables the seamless integration of scientific updates provided by the GEOS-Chem CTM community into GEOS-CF without the need to make any modifications to the source

code. The scientific validity of the GEOS-Chem chemistry module within GEOS has been demonstrated by Hu et al. (2018), who show that a one-year global simulation of atmospheric composition at 12.5 km^2 produces results consistent with the offline GEOS-Chem model. GEOS-CF is a natural extension of the online GEOS-Chem module embedded in GEOS, with a focus on daily operation and forecast capabilities.

GEOS-CF is the latest in a series of research and applications products generated by the NASA Global Modeling and Assimilation Office (GMAO), including the GEOS forward processing weather and aerosol system (GEOS FP), GEOS FP for instrument teams (GEOS FP-IT, Lucchesi, 2015), the second Modern-Era Retrospective analysis for Research and Applications (MERRA-2, Gelaro et al., 2017), and the Seasonal to Subseasonal Forecasting System (GEOS-S2S, Borovikov et al., 2019; Molod et al., 2020). It leverages GMAO's model infrastructure and directly builds on a number of development activities centered around the GEOS model, with the goal to extend these forecasting capabilities toward (short-lived) trace gases and aerosols.

GEOS is a General Circulation Model (GCM) and Data Assimilation System (DAS) consisting of a suite of model components that can be connected in a modular manner through the Earth System Modeling Framework (ESMF, Hill et al., 2004) and Modeling Analysis and Prediction Layer (MAPL, Suarez et al., 2007) software interface. The model can be configured to run with fully interactive chemistry so that the chemical constituents feed back to the dynamics ('online'), or as an offline model where external meteorological fields are used as input. A hybrid approach is the 'replay' feature, where the model dynamics are nudged toward pre-computed analysis fields (from a previous DAS simulation) in a way that is consistent with the internal physics of the model (Orbe et al., 2017). This approach is particularly useful for chemistry simulations as it sidesteps the need to conduct a computationally costly meteorological data assimilation cycle. Several chemistry and aerosol modules of varying complexity are available in GEOS (Nielsen et al., 2017), enabling a wide range of applications including: near real-time simulation of aerosols using the GOCART module (Colarco et al. 2010; Randles et al., 2017; Buchard et al., 2017), computationally efficient analysis of stratospheric ozone using parameterized chemistry in combination with 3D-Variational assimilation of satellite observations (Wargan et al., 2015); multi-decade simulation of tropospheric and stratospheric chemistry using the Global Modeling Initiative (GMI) chemistry module (Douglass et al., 2004; Duncan et al., 2007, Strahan et al., 2007); and fully coupled simulation of gas-phase and aerosol chemistry using the GEOS-Chem chemistry module embedded in GEOS (Long et al., 2015).

In this paper we describe the configuration of GEOS-CF version 1.0 (Section 2) and demonstrate the validity of the produced analyses through comparison against independent observations (Sections 3-4). Model forecasts are evaluated in Section 5 and we discuss how model skill scores can be improved by applying a bias-correction to the surface observations using a machine-learning approach. As described in detail below, the current version of GEOS-CF constitutes a hybrid model between an online weather and chemistry assimilation system and an offline CTM application, with a development pathway toward a fully coupled forecasting system with integrated trace gases and aerosols. Many of its design features were guided by practical considerations as well as computational limitations related to the simulation of atmospheric chemistry.

2 Model Description

2.1. General Description

A schematic of the GEOS-CF v1.0 modeling system is provided in Figure 1. GEOS-CF is operated in near real-time, producing a 5-day forecast once a day. The forecast initial conditions are provided by a one-day replay simulation (i.e., 'analysis') constrained by pre-computed meteorological analysis fields. In the v1.0 configuration, the analysis forcings that GEOS-CF uses are GEOS FP-IT meteorological variables and GOCART aerosols providing meteorological feedbacks, and GEOS-FP stratospheric ozone (described below). All other trace gases are integrated without observational constraints. The resulting model conditions at the end of the simulated day also serve as input for the next day's replay step (i.e., restart files). This preserves the model chemical and meteorological state from one forecast cycle to the next, leading to a continuous atmospheric composition archive since January 2018.

GEOS FP-IT is a 'frozen' model system that is comparable to MERRA-2 but - unlike MERRA-2 - is available in near real-time to support retrievals by satellite instrument teams. The GEOS model in general, and version of the GEOS GCM used by GEOS FP-IT (v5.12.4) in particular, has shown to be well suited for atmospheric chemistry applications as it realistically captures features critical to atmospheric composition, such as the seasonal climate of moisture and temperature and large-scale transport of constituents (e.g., Pawson et al., 2007; Douglass et al., 2014; Oman and Douglass, 2014; Molod et al., 2015; Gelaro et al., 2017).

GEOS-CF v1.0 uses a model physics package that is similar to MERRA-2 and GEOS FP-IT, consisting of the GEOS atmospheric model, version 5, described in Rienecker et al. (2008) with updates as described in Molod et al. (2012) and Molod et al. (2015). The model uses the finite-volume dynamical core of Lin (2004) with a cubed sphere grid discretization to avoid grid-cell singularities (Putman and Lin, 2007). It is run at cubed-sphere c360 horizontal resolution (roughly equivalent to 0.25° x 0.25°) and 72 hybrid-eta levels from the surface to 0.01 hPa. Model physics includes parameterizations for moist processes, radiation, turbulent mixing, land-surface processes, and gravity wave drag. The moist module contains parameterization of convection using the Relaxed Arakawa-Schubert scheme (Moorthi & Suarez, 1992), and the single-moment parameterization for large-scale precipitation and cloud cover described in Bacmeister et al. (2006). The radiation module includes parameterization for long-wave (Chou 1990, 1992) and short-wave radiation processes (Chou and Suarez 1994). Turbulence is parameterized using the gradient Richardson number in the free atmosphere and the Lock scheme (Lock et al., 2000) interfaced with the scheme of Louis and Geleyn (1982) in the boundary layer. Exchange of heat, moisture and momentum between land, atmosphere, and ocean or sea ice surfaces are parameterized using Monin-Obukhov similarity theory (Helfand and Schubert, 1995, Molod et al., 2013), and the gravity wave drag parameterization contains orographic (McFarlane, 1987) and non-orographic (Garcia & Boville, 1994) waves.

In the GEOS-CF system, the GEOS physics components are coupled to the GOCART aerosol component to provide consistent physics with the GEOS FP-IT meteorology. The GEOS-Chem chemistry module is run "passively" to provide coupled aerosol-oxidant chemistry in the troposphere and stratosphere (Hu et al., 2018). The GOCART aerosols, constrained during the replay step by aerosol optical depth (AOD) observations from the Moderate Resolution Imaging Spectroradiometer (MODIS) aboard the Terra and Aqua satellites (Randles et al., 2017), are used

to compute the feedback between aerosols and dynamics. This ensures consistency between GEOS-CF and the GEOS FP-IT analysis fields. Currently, there is no chemical coupling between GOCART and GEOS-Chem, and no observations are directly assimilated into GEOS-CF. However, stratospheric ozone in GEOS-Chem is nudged towards ozone produced by GEOS FP, which is constrained by ozone measurements from the Microwave Limb Sounder (MLS), Ozone Monitoring Instrument (OMI), and NASA's Ozone Mapping and Profiler Suite (OMPS) and produces a realistic analysis of ozone in the stratosphere (Wargan et al., 2015; 2020). In addition, near real-time MODIS observations of fire radiative power are used to constrain fire emissions, as produced by the Quick Fire Emissions Dataset (QFED) (Darmenov and Da Silva, 2015).

All computations are conducted on the Discover supercomputing cluster of the NASA Center for Climate Simulation (NCCS). Run on 3510 Intel Xeon Haswell processor cores, the one-day analysis and 5-day forecast takes approximately 8.5 wall-clock hours. GEOS-CF analysis and forecast output includes chemistry and meteorology "surface" output every 15 minutes as well as hourly-average and instantaneous fields for surface, column-average, and 3-dimensional model output. The model output is publicly available at https://gmao.gsfc.nasa.gov/weather_prediction/GEOS-CF/data_access/ in the form of on-demand figures or through access to the model output (in netCDF data format) via Hypertext Transfer Protocol (HTTP) file download or through the Open-source Project for a Network Data Access Protocol (OPeNDAP) remote access tool. The full 5-day model forecast output is publicly available for a duration of 14 days. Given the growing interest in air quality forecasting applications, the model forecasts for a selection of surface air pollutants are made available on the public portal indefinitely. Full details on available output and data access are available in the GEOS-CF File Specification document (Knowland et al., 2020).

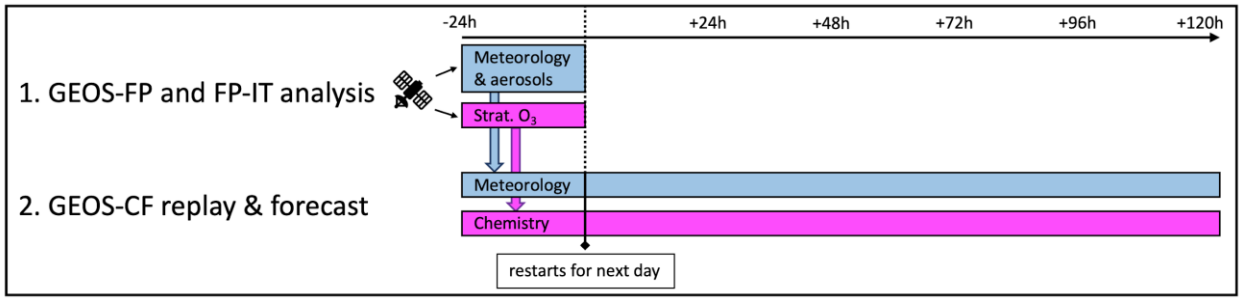

Figure 1. Schematic of the GEOS-CF modeling system approach, consisting of one day analysis and 5-day forecast. This combination of simulations is conducted on a daily basis.

2.2. Chemistry

GEOS-CF v1.0 uses the continually updated standard version of the GEOS-Chem chemistry module to simulate coupled aerosol-oxidant chemistry in the troposphere and stratosphere. The current version 12.9.2 of GEOS-Chem has been implemented into GEOS-CF as of this writing, but results are presented here for version 12.0.1 in order to have a two-year record for comparison to observations. GEOS-Chem is ESMF-compliant and its chemistry module is implemented here as an ESMF gridded component of GEOS, as described in Long et al. (2015) and Hu et al. (2018).

The gas-phase chemistry scheme includes detailed tropospheric chemistry of HO_x, NO_x, BrO_x, volatile organic compounds (VOC), and O_3, as originally described by Bey et al. (2001), with addition of halogen chemistry by Parrella et al. (2012) and Sherwen et al. (2016) plus updates to

isoprene oxidation as described by Mao et al. (2013) and Miller et al. (2017). Stratospheric chemistry is fully coupled with tropospheric chemistry through the Unified tropospheric-stratospheric Chemistry eXtension (UCX, Eastham et al. (2014)) and extends to the top of the atmosphere. Photolysis rates are computed by GEOS-Chem using the Fast-JX code (Bian and Prather, 2002). The gas-phase mechanism comprises 250 chemical species and 725 reactions and is solved using the Kinetic PreProcessor KPP Rosenbrock solver (Sandu and Sander, 2006). The aerosol simulation includes sulfate-nitrate-ammonia chemistry (Park et al., 2004), black carbon (Park et al., 2003; Wang et al., 2014), organic aerosols (Marais et al., 2016), mineral dust (Fairlie et al., 2007; Ridley et al., 2012), and sea salt aerosols (Jaeglé et al., 2011). Aerosol and gas-phase chemistry interact through gas-aerosol partitioning (Fountoukis and Nenes, 2007; Pye et al., 2009), heterogeneous chemistry on aerosol surface (Evans and Jacob, 2005; Mao et al., 2013), and aerosol impacts on photolysis (Martin et al., 2003). Methane concentrations are prescribed as monthly mean surface concentrations, spatially interpolated from NOAA GLOBALVIEW flask data (Dlugokencky et al., 1995).

2.3. Emissions and Deposition

The dry deposition scheme in GEOS-Chem is based on the resistance-in-series model of Wesely (1989). Wet deposition of aerosols and soluble gases includes scavenging in convective updrafts, in-cloud rainout, and below-cloud washout (Liu et al., 2001; Amos et al., 2012). All emission calculations are done using the Harmonic Emissions Component HEMCO v2.1.009 (Keller et al., 2014). Table 1 summarizes the emission configuration used by GEOS-CF v1.0. Anthropogenic emissions are broken down into hourly values using sector-specific day-of-week and diurnal scale factors (van der Gon et al., 2011). In addition, an annual gridded scale factor based on the Open-source Data Inventory for Anthropogenic CO_2 (ODIAC; Oda et al., 2017) is applied to the anthropogenic emissions of CO.

Table 1. *Emissions used by GEOS-CF.*

Description	**Reference**	**Comments**
Offline inventories		
Anthropogenic NO, CO, black carbon (BC), organic carbon (OC), Ammonia (NH_3)	HTAP v2.2 (Janssens-Maenhout et al., 2015)	Global except Africa
Anthropogenic SO_2	OMI-HTAP (Liu et al., 2018)	Global except Africa
Anthropogenic VOCs	RETRO (Schultz et al., 2008)	Global except Africa
Anthropogenic NO, CO, SO_2, BC, OC, NH_3, VOCs	DICE-Africa (Marais and Wiedinmyer, 2016)	Africa
Arctic seabird NH_3	Croft et al. (2016)	
Volcanic SO_2	Carn (2019)	5% of the sulfur emitted as SO_4
Aircraft NO_x, CO, SO_2, VOCs, BC, OC	AEIC (Stettler et al., 2011)	
Dynamic emissions		
Biogenic VOCs	MEGAN v2.1 (Guenther et al., 2012)	
Biomass burning NO_x, CO, SO_2, VOCs, BC, OC	QFED v2.5 (Darmenov and da Silva, 2015)	35% emitted between 3.5 and 5.5 km altitude (Fischer et al., 2014).
Lightning NO_x	Murray et al., 2012	
Soil NO_x	Hudman et al., 2012	
Soil dust	Zender et al., 2003	

Sea salt aerosols	Gong, 2003; Jaeglé et al., 2011	
Oceanic DMS, CH_2O, C_3H_6O	Johnson, 2010; Nightingale et al., 2000	
Oceanic iodine	Carpenter et al., 2013	

3 Observations used for Model Evaluation

GEOS-CF is intended to supplement NASA's broad range of space-based and in-situ observations, providing a new tool for researchers, government scientists, and air quality managers. We therefore focus our evaluation on the species most pertinent to these applications, including O_3, NO_2, CO, and aerosols. These species are also constantly evaluated by the broader GEOS-Chem community using the standard CTM simulations (e.g., Hu et al., 2017, 2018; Travis et al., 2019). However, it should be noted that GEOS-CF simulations can differ from standard GEOS-Chem simulations due to the higher horizontal resolution and differences in the emission inputs, in particular wildfire emissions (Hu et al., 2018).

We first evaluate the ability of the GEOS-CF analysis to provide a realistic representation of atmospheric composition based on the hourly-average analysis fields (Section 4). Differences between the 5-day model forecasts and the model analysis are discussed in Section 5.

The data sets used for model validation are summarized in Table 2. Briefly, we evaluate the global tropospheric distribution of O_3 against ozonesonde observations obtained from the World Ozone and Ultraviolet Data Center (WOUDC, http://www.woudc.org), NO_2 against the OMI NASA standard tropospheric column NO_2 product v4.0 (Lamsal et al., 2020), CO total columns against satellite retrievals from the Measurements Of Pollution In The Troposphere (MOPITT) V8 (Deeter et al., 2019), and AOD against the Aerosol Robotic Network (AERONET) level 2.0 daily average data from the version 3 data product (https://aeronet.gsfc.nasa.gov/; Giles et al., 2019). In addition, we compare simulated surface concentrations against in-situ observations from the Global Atmospheric Watch (GAW) World Data Center for Greenhouse Gases (WDCGG, https://gaw.kishou.go.jp/) and World Data Centre for Reactive Gases (WDCRG, https://www.gaw-wdcrg.org/), as well as observations from the OpenAQ database (https://openaq.org). For NO_2, we omitted mountainous GAW sites given that the model resolution of 25x25 km^2 is not high enough to resolve the fine-scale vertical gradients around mountain slopes. On average, the depth of the GEOS-CF model surface layer is 130 meters and we use this value without attempting to adjust for sub-grid vertical gradients (Travis et al., 2019). All aerosol evaluation is based on the GEOS-Chem aerosols, and model $PM_{2.5}$ is calculated for a relative humidity (RH) of 35%. The validation covers the time period from the start of the GEOS-CF data record on Jan 1, 2018 to Dec 31, 2019.

Figure 2 shows the global distribution of all in-situ observations used in the evaluation. The GAW observation sites are located away from the major pollution sources, representing the global background concentrations. In contrast, most observations available on the OpenAQ platform are located in densely populated areas, providing information about local air pollution. For our analysis, we only include OpenAQ locations with at least 80% of data coverage during the 2-year period. The OpenAQ and AERONET observations are further grouped into six geographical regions, as shown in Figure 2. This subset of observations provides good coverage for North America, Europe, and Eastern Asia (especially China) but a limited view of other

304 regions such as South America or Africa. For those under-represented regions, our analysis relies
305 heavily on the global daily satellite observations.
306
307 **Table 2.** *Overview of observation data sets used for GEOS-CF model validation*

Description	Species	# sites	Reference
Ozonesonde	O_3	24	Thompson et al., 2017
NASA OMI NO_2 v4.0	Tropospheric NO_2	global	Lamsal et al., 2020
MOPITT v8	Total CO	global	Deeter et al., 2019
AERONET	AOD at 550nm	195	Giles et al., 2019
GAW WDCGG	CO	54	https://gaw.kishou.go.jp/
GAW WDCRG	O_3, NO_2	48 (O_3), 6 (NO_2)	https://www.gaw-wdcrg.org/

308

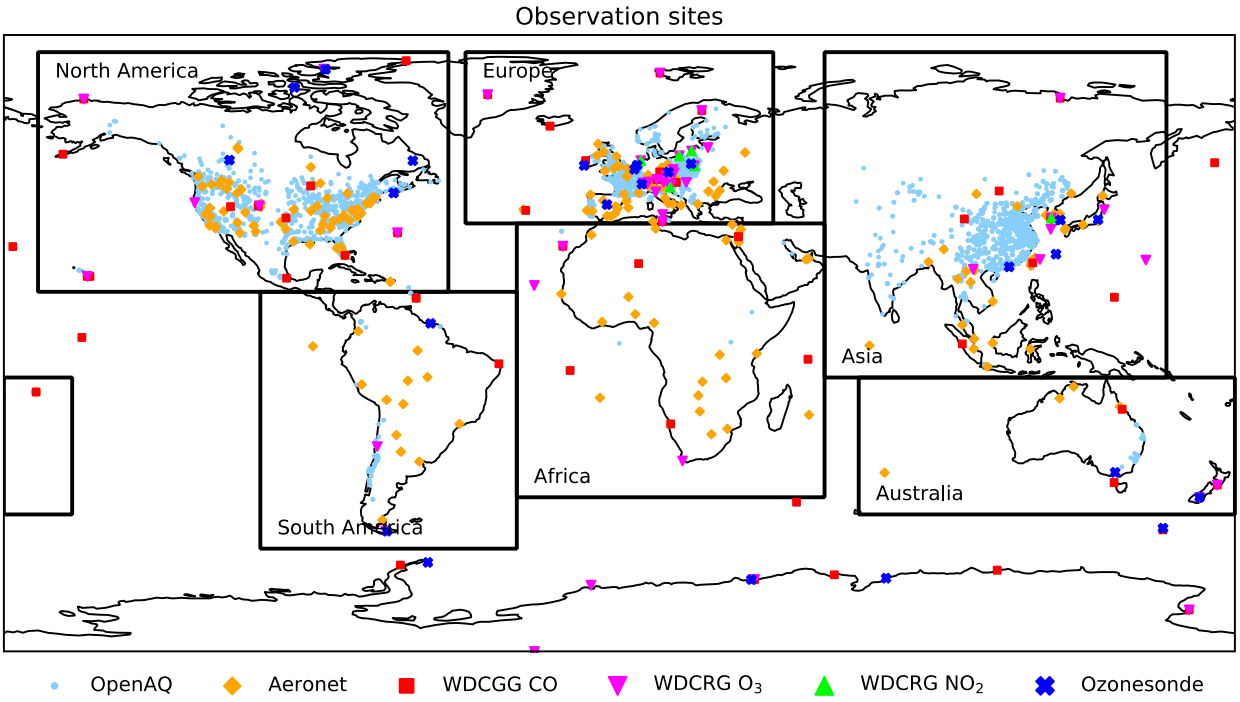

309
310 **Figure 2.** Overview of observation sites used for model validation. Black boxes show the six
311 regions used for aggregation of OpenAQ and Aeronet observations.

312 ## 4 Evaluation of Model Analysis

313 ### 4.1. Model Skill Scores

314 We first highlight the model skill scores against all surface observations before
315 discussing the individual species in more detail below. Figure 3 shows monthly model skill
316 scores for O_3, NO_2, CO, and $PM_{2.5}$ and/or AOD, aggregated by observation type. The skill scores

used are the normalized mean bias (NMB), normalized root mean square error (NRMSE), and Pearson correlation coefficient (R):

$$NMB = \frac{\Sigma_{n=1}^{N}(y_n - o_n)}{\underline{o}} \quad (1)$$

$$NRMSE = \frac{\sqrt{\frac{1}{N}\Sigma_{n=1}^{N}(y_n - o_n)^2}}{o_{0.95} - o_{0.05}} \quad (2)$$

$$R = \frac{\Sigma_{n=1}^{N}(y_n - \bar{y})(o_n - \bar{o})}{\sqrt{\Sigma_{n=1}^{N}(y_n - \bar{y})^2}\sqrt{\Sigma_{n=1}^{N}(o_n - \bar{o})^2}} \quad (3)$$

where y_n denotes an indidivual model estimate, $\bar{y}$ is the model average, o_n is the observation associated with y_n, and $\bar{o}$ is the observation average; $o_{0.05}$ and $o_{0.95}$ are the 5th and 95th percentile, respectively, of the observations sample, and N is the total number of hourly observation-model pairs.

For hourly average surface O_3, the model shows a normalized mean annual bias of -0.015 compared to the GAW sites, with little seasonal variability (Figure 3). The GAW sites are typically located in remote locations and the small model bias indicates that the model adequately captures atmospheric background O_3 throughout the year. This is confirmed by the low NRMSE of 0.12 and the correlation coefficient of 0.66, again with small seasonal variability. Compared to the GAW sites, the simulated O_3 shows weaker skill scores relative to the OpenAQ observations with an NMB of 0.13, an NRMSE of 0.43 and R of 0.49. As further discussed below, the OpenAQ comparisons highlight a pronounced model overestimation of surface O_3 during the summer months, especially over North America.

For NO_2 (second column of Figure 3), the normalized model bias is -0.06 compared against the GAW sites, and -0.30 against the OpenAQ sites. The model shows a strong seasonal change in the NMB at the GAW sites, where the model on average overpredicts wintertime NO_2 by up to 30% but underpredicts spring and early summer concentrations by a similar amount. The OpenAQ bias shows the opposite direction with a reduction of the negative bias from -0.4 during winter to -0.25 during summer. The NRMSE is 0.15 at the GAW sites and 0.48 at the OpenAQ sites, similar to O_3. The R values for NO_2 are the lowest for all analyzed species, with an average score of 0.27 and 0.29 at the GAW and OpenAQ sites, respectively. Apart from potential NO_2 observation interference with other nitrogen compounds (Winer et al., 1974; Grosjean and Harrison, 1985; Steinbacher et al., 2007), we attribute this to the short atmospheric lifetime of NO_2, which makes it challenging for the model to capture the hourly variability in surface NO_2 in full detail.

The simulated CO compares well against the 54 GAW sites, with an NMB of -0.036, an NRMSE of 0.088 and R of 0.74. The model error is largest during the NH summer months, with a decrease in NMB to -0.14, an increase in NRMSE to 0.18, and a reduction of R to 0.5.

The model comparisons against AERONET AOD and OpenAQ $PM_{2.5}$ observations reveal a systematic model overestimation of aerosol concentrations in GEOS-CF, with an average NMB of 0.61 for AOD and 1.6 for surface $PM_{2.5}$. Known model issues in the treatment of model emissions and wet scavenging contribute to these biases, as will be discussed in more detail below. In addition, some $PM_{2.5}$ observations on the OpenAQ platform represent dry particulate matter while model $PM_{2.5}$ assumes 35% RH, which also contributes to the mismatch. At the AERONET sites, the model shows a good correlation score of 0.71 and the NMRSE of 0.15 is comparable to that of other species at background sites, indicating that the model captures the

relative changes in AOD well despite the high model bias. For surface $PM_{2.5}$, the average model NRMSE is 1.34 and R skill score is 0.35.

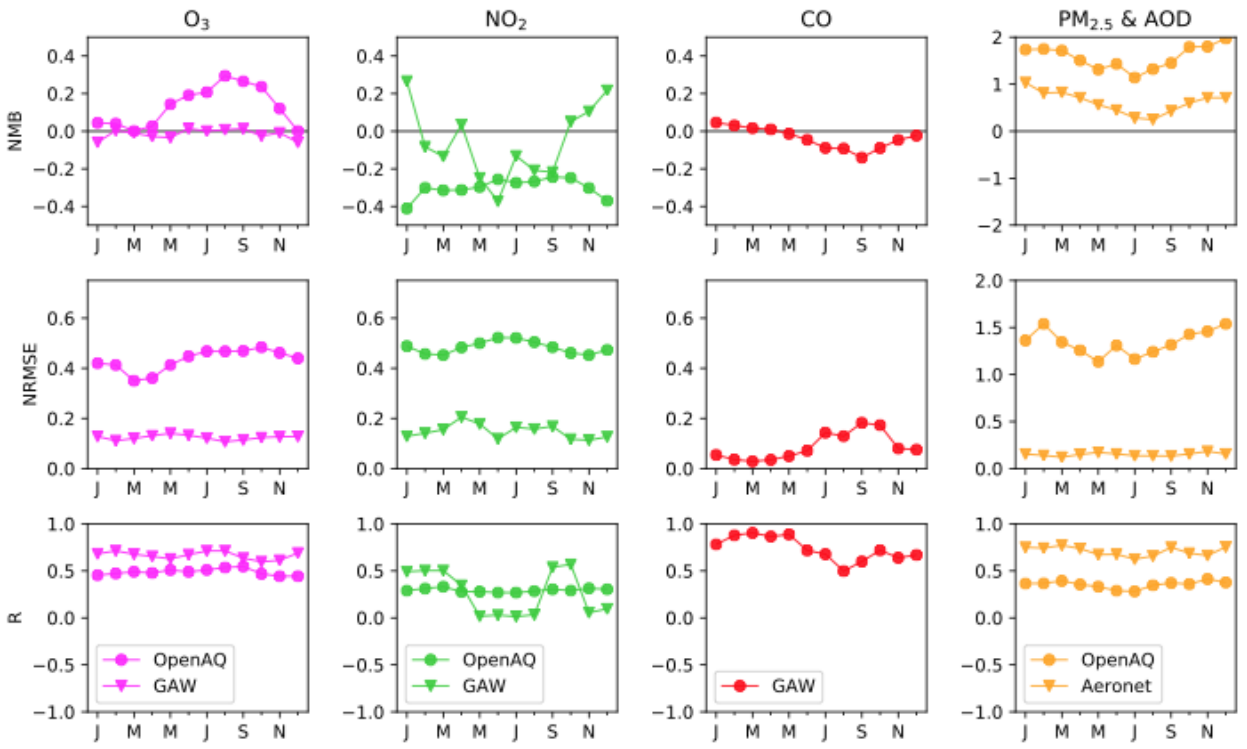

Figure 3. Overview of NMB, NRMSE and R for O_3, NO_2, CO, and $PM_{2.5}$ (OpenAQ only) and AOD (Aeronet only). Shown are the monthly skill score means aggregated by observation type. Note the different scale for $PM_{2.5}$ and AOD.

4.2. Ozone

Comparisons of GEOS-CF against ozonesondes and GAW surface observations show that GEOS-CF reproduces well-known features of background surface ozone, such as the local maxima in the Northern Hemisphere (NH) during spring.

Figure 4 shows annual mean (2018-2019) vertical ozone profiles as observed by ozonesondes at 24 locations across the world (see Figure 2 for locations), compared against corresponding GEOS-CF model concentrations. While GEOS-CF generally captures the observed vertical structure of ozone, the model tends to underestimate free tropospheric ozone (approx. 800-300 hPa) over the NH midlatitudes. For these profiles (e.g., De Bilt, Payerne, Madrid, Tateno), the simulated vertical gradient is much less pronounced than observed and the model consistently underestimates ozone concentrations. This pattern is consistent with previous comparisons of the online GEOS-Chem module against observations (Hu et al., 2018) and implies two potential model errors: (1) excessive vertical mixing resulting in an overestimation in the lower altitudes and underestimation at higher altitudes, as evident over Payerne, Yarmouth, and Madrid (Figure 4); and (2) an underestimation of lightning NO_x over the NH midlatitudes, resulting in an underestimation of ozone production in the upper troposphere. The global lightning NO_x source in GEOS-CF is 5.9 Tg N yr^{-1}, in good agreement with other studies (Schumann and Huntrieser, 2007) and the 6.0 Tg N yr^{-1} reported for the GEOS-Chem CTM (Murray et al., 2012). However, due to the real-time nature of the system, the GEOS-CF

lightning parameterization uses the unconstrained cloud top height parameterization (Price and Rind, 1992; 1993; 1994) and does not apply time-dependent, regional redistribution factors based on Lightning Imaging Sensor (LIS) and the Optical Transient Detector (OTD) satellite observations as is standard in GEOS-Chem. As described in Murray et al. (2012), this results in an underestimation of simulated lightning flash rates over the Northern extratropics, which is likely one of the main reasons for the model underestimation of ozone in the NH upper troposphere. We also note that the model vertical resolution is approx. 500m (20 hPa) in the mid- to upper troposphere, which might be insufficient to resolve the strong vertical gradients across the tropopause boundary and contribute to the model-observation mismatches in the upper troposphere. Over the Southern Hemisphere (SH), the simulated ozone profiles are in good agreement with the ozonesonde observations and show an improved O_3 distribution compared to the offline GEOS-Chem model (Hu et al., 2018).

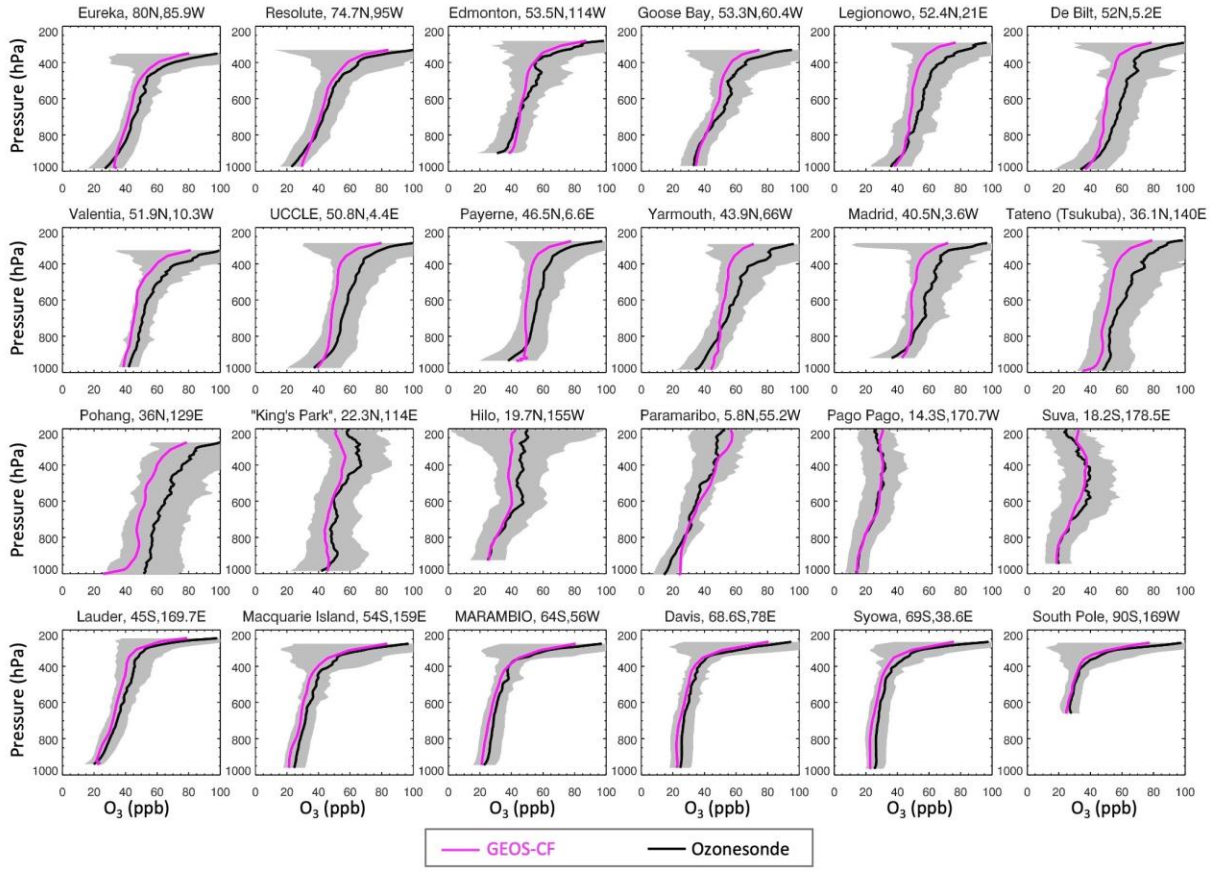

Figure 4. Vertical profile of annual average ozone (2018-2019) at 24 sites as observed by ozonesondes (black) and simulated by GEOS-CF (magenta). The grey shaded area indicates sonde observation standard deviation.

The GAW observations show a pronounced seasonal cycle for surface O_3 with a maximum of 30-50 ppbv during spring and summer and a low of 10-30 ppbv in winter, a feature that is well reproduced by GEOS-CF (Figure 5). At remote locations such as the high-latitude GAW sites (Figure 5 top row), the seasonal cycle is more distinct with a peak in early spring. The ozone maximum develops more slowly at locations that are more heavily influenced by anthropogenic emissions. As already observed in the ozonesondes, the model underestimates

ozone over the Southern Ocean by up to 10 ppbv. This is likely due to excessive ozone deposition over seawater (Pound et al., 2020), a problem since corrected in newer versions of GEOS-Chem.

Figure 6 shows monthly average surface ozone by region, as captured by observations in the OpenAQ database and simulated by GEOS-CF. The model generally overestimates surface O_3 over Europe, North and South America and Australia by 5-10 ppbv and underestimates it over Africa and Asia by up to 20 ppbv. The model-observation mismatch is larger than for the remote GAW sites, suggesting that sub-grid factors such as vertical and horizontal model representation errors and nighttime loss of ozone by reaction with NO contribute to this difference (Travis et al., 2019; Dacic et al., 2020). Models generally underestimate ozone nighttime depletion (Travis et al., 2017) and evaluation of surface ozone is thus often restricted to daytime ozone (Hu et al., 2018, Travis et al., 2019). As shown in Figure 7, restricting the analysis to daytime ozone (12:00 to 16:00 local time) does indeed improve the comparison and reduce the bias by up to 5 ppbv, in particular over Europe, South America and Australia. The model still shows a systematic positive bias over the US during summer and fall, a known issue in GEOS-Chem (Travis et al., 2017, Hu et al., 2018).

Factors that likely contribute to the high NH surface ozone in GEOS-CF are uncertainties in the production of ozone from the oxidation of isoprene (Travis et al., 2016; Bates et al., 2019) and errors in ozone deposition to wet surfaces (Travis et al., 2019). In addition, most OpenAQ observation sites are located near densely populated areas, and the 25x25 km^2 model simulation cannot fully capture the fine-scale features characteristic for these environments (Keller et al., 2020).

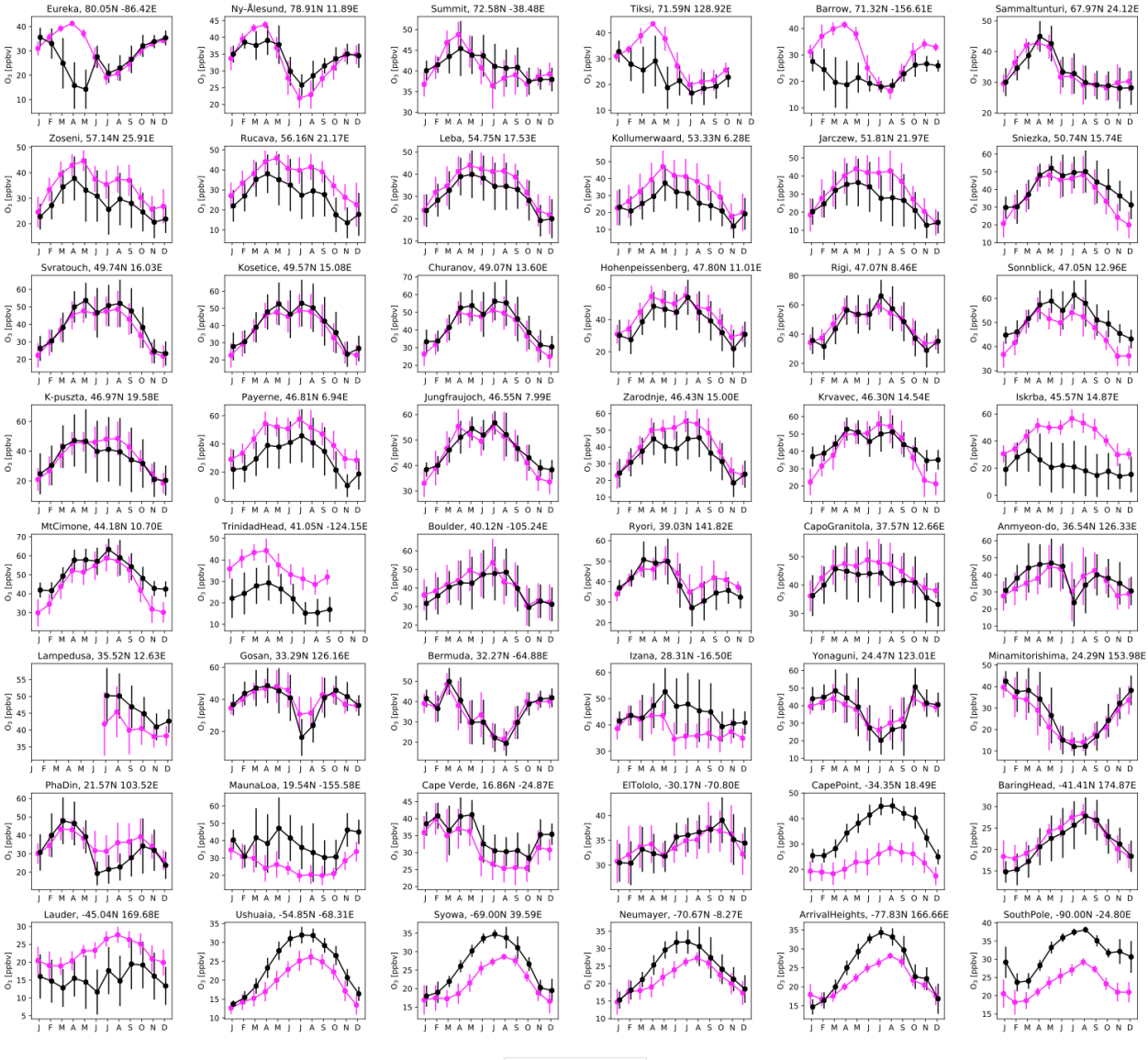

Figure 5. Monthly average surface O_3 as observed at 48 GAW sites (black) and simulated by GEOS-CF (magenta). Vertical bars represent the standard deviation of hourly variability. Y-axis ranges vary by station.

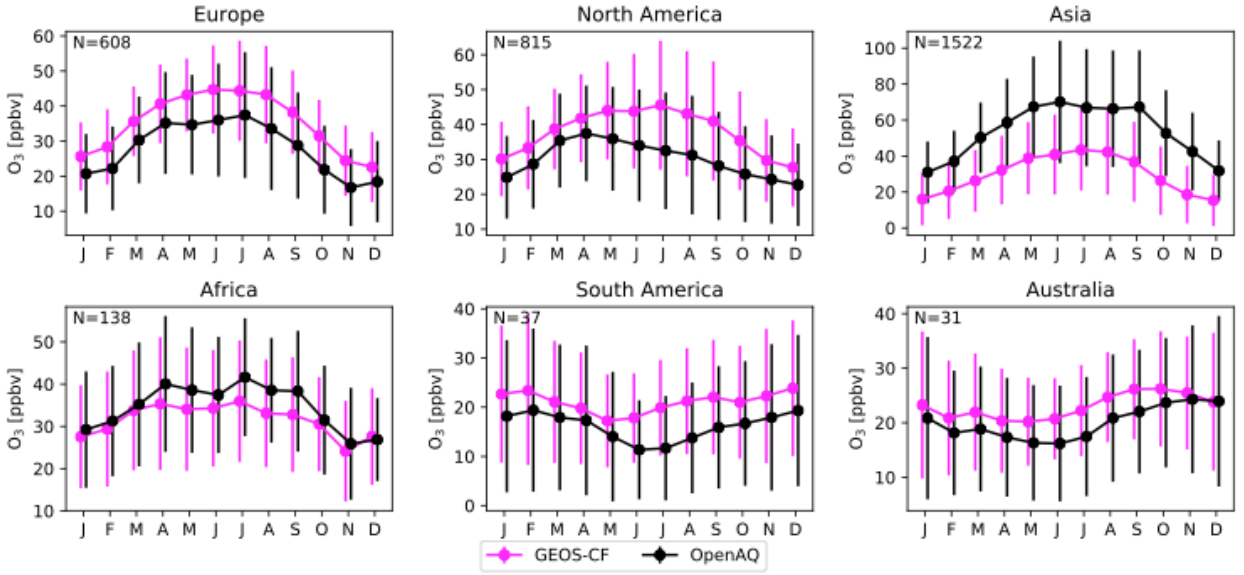

Figure 6. Monthly average surface O_3 grouped into six regions as obtained from the OpenAQ database (black) and simulated by GEOS-CF (magenta). Vertical bars represent the standard deviation of hourly variability across all sites. Number of sites is given in the inset. Y-axis ranges vary by region.

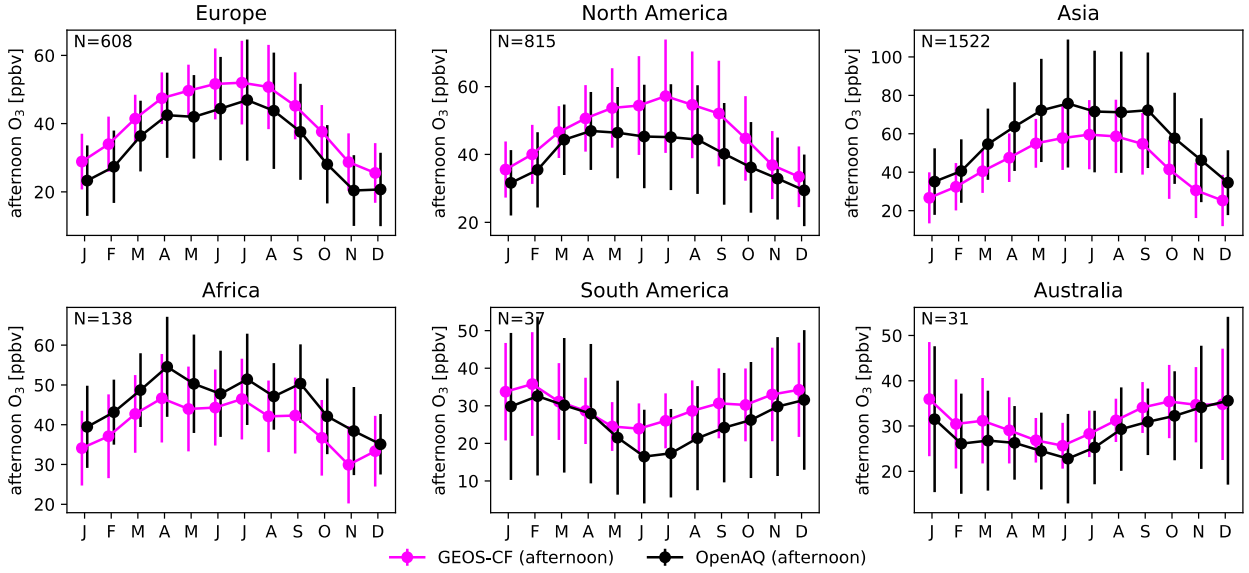

Figure 7. As Figure 6 but using afternoon ozone only (12:00-16:00 local time).

4.3. Nitrogen Dioxide

As shown in Figure 8, GEOS-CF captures major features of the global distribution of tropospheric NO_2. The model simulated NO_2 columns (Figure 8a) show distinct hot spots over urban areas (Eastern China, Europe, Eastern US), reflecting the dominant contribution of fossil fuel combustion coupled with the short atmospheric lifetime of NO_2 (Streets et al., 2013, Duncan et al., 2016). Additional hot spots resulting from biomass burning are found over Africa and the boreal region of Canada (Figure 8a). The spatial pattern simulated by GEOS-CF agrees well with the NO_2 columns observed by OMI. Over Eastern China, the model simulated NO_2 columns are

up to $3.0x10^{15}$ molecules cm^{-2} (or approx. 40%) higher than the OMI observations (Figure 8b), suggesting a potential overestimation of NO_x emissions or a longer NO_x lifetime in the model (Shah et al., 2020). However, the OMI retrieval algorithm v4.0 tends to underestimate tropospheric NO_2 over polluted areas (Lamsal et al., 2020), which complicates the analysis. As further discussed in the next section, the comparison against surface observations does not support the view of a broad-based overestimation of surface NO_2 over Asia.

As shown in Figure 8c, the simulated seasonality of tropospheric NO_2 columns is in good agreement with OMI observations. Over areas dominated by anthropogenic activities, such as the US, Europe, and China, the simulated NO_2 columns show a distinct seasonal cycle with the minimum during summer and peak during winter, driven by the seasonal variation in NO_x lifetime against oxidation (Shah et al., 2020). The seasonal cycle observed over China is well captured by GEOS-CF, while the simulated wintertime peak over the US and Europe is higher than observed by OMI. Chemical loss of NO_x during winter is dominated by N_2O_5 hydrolysis, which is sensitive to NO_x emissions and ozone concentrations (Jaeglé et al, 2018; Shah et al., 2020). Over Africa, the seasonal cycle is dominated by summer biomass burning, which is well captured by the model.

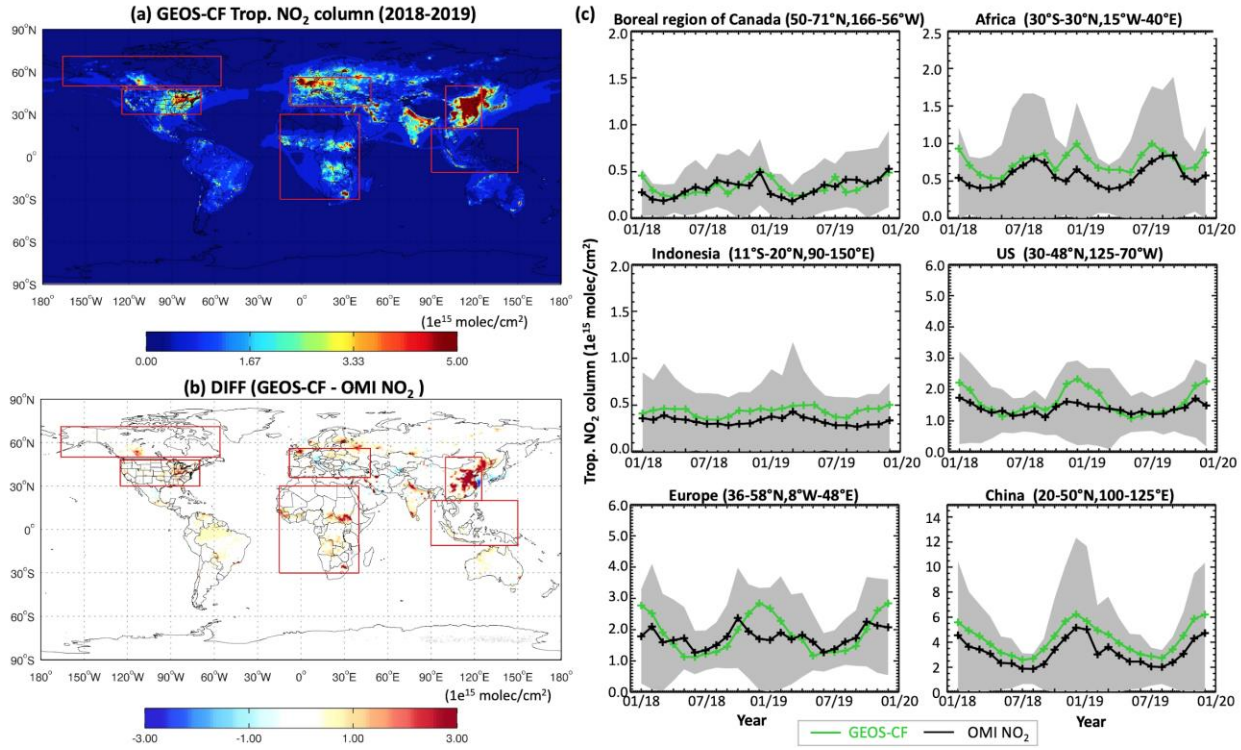

Figure 8. Comparison of GEOS-CF against OMI tropospheric column NO_2. **a)** the 2018-2019 average tropospheric NO_2 column (1-2pm local time) as simulated by GEOS-CF. **b)** the difference between model simulated tropospheric column and NASA OMI NO_2 (v4.0) observations. **c)** Right panel shows the tropospheric NO_2 time series averaged for six regions, as shown in **a** and **b** (n.b., y-axis intervals are not the same for each time-series).

Figure 9 shows comparisons of monthly mean surface NO_2 at 6 GAW sites (n.b., all located in Europe) against model simulated concentrations. These comparisons show that GEOS-CF is in good agreement with the (non-mountainous) GAW sites, suggesting that it provides a

realistic simulation of background surface NO_2 over Europe. Figure 10 further evaluates the simulated distribution of global surface NO_2 in comparison to observations in OpenAQ. The model is in excellent agreement with observations over North America and Africa but underestimates concentrations over Europe and South America, as well as Asia during the wintertime. The apparent low bias over Europe and Asia is inconsistent with the tropospheric column comparisons shown in Figure 8 and also the comparison against the GAW observations (Figure 9), which do not show such a systematic underestimation of NO_2 by GEOS-CF.

The comparison of surface concentrations of NO_2 is complicated by the fact that most surface observations are based on chemiluminescence using a molybdenum converter, which can result in an overestimation of reported NO_2 concentrations due to interference with other oxidized nitrogen compounds (Winer et al., 1974; Grosjean and Harrison, 1985; Steinbacher et al., 2007). This might explain some of the model underestimation of NO_2 relative to the OpenAQ observations. In addition, since the OpenAQ observations tend to be located in relative proximity to urban areas they often do not represent the regional average NO_2 concentrations captured by GEOS-CF, which can introduce a systematic bias. While this is an issue for all analyzed species, the problem is particularly pronounced for NO_2 given its large spatial and temporal variability.

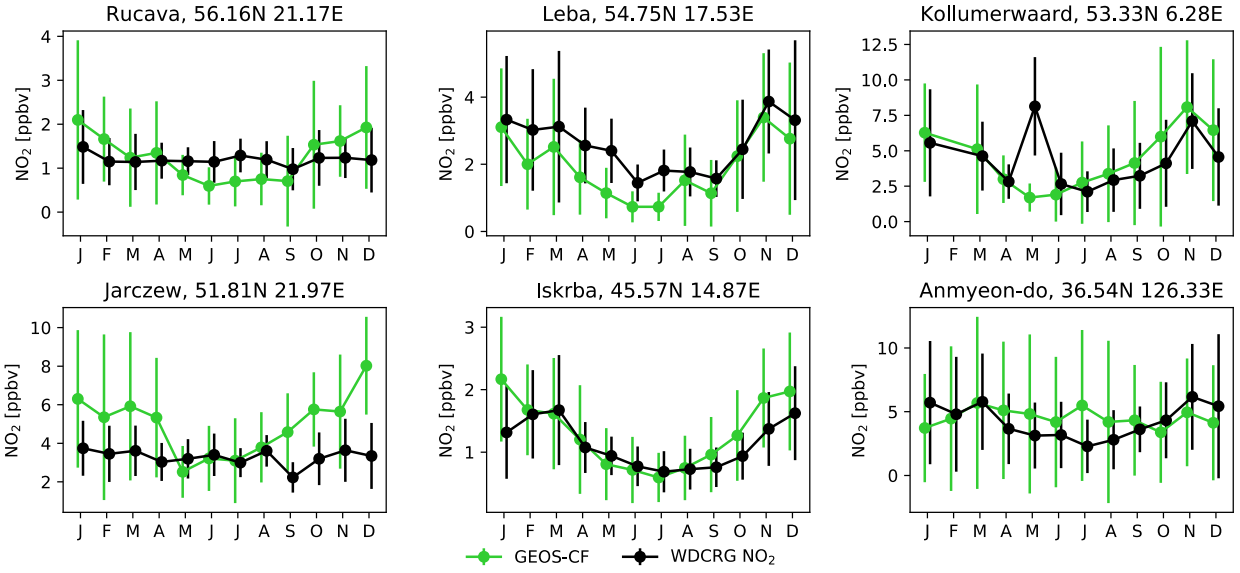

Figure 9. Monthly average surface NO_2 as observed at 6 GAW sites (black) and simulated by GEOS-CF (green). Vertical bars represent the standard deviation of hourly variability. Y-axis ranges vary by station.

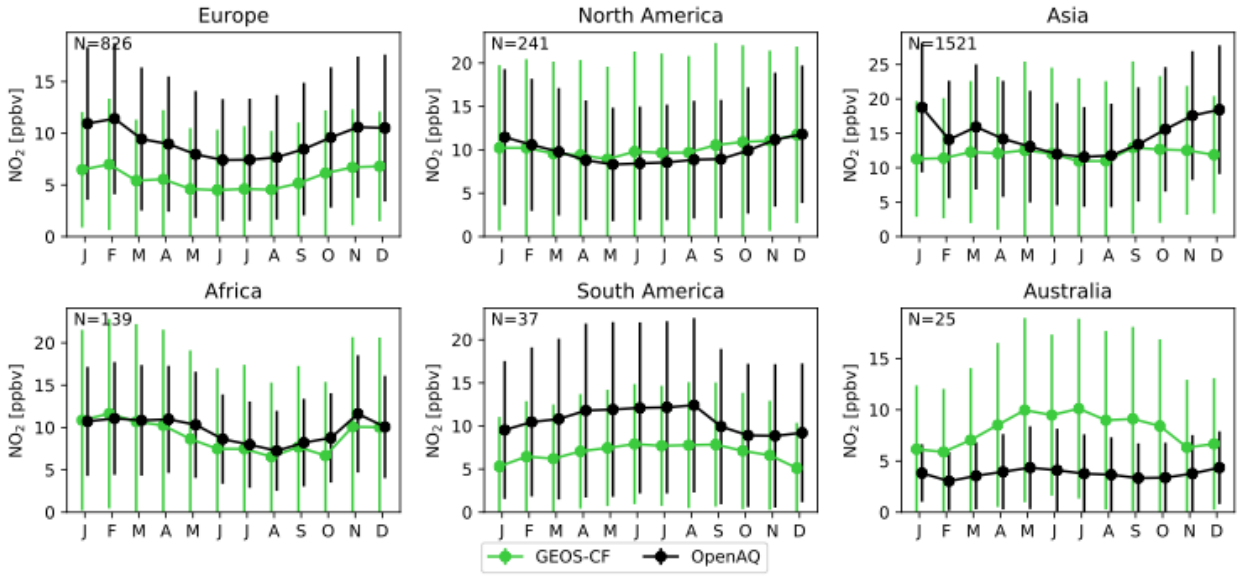

Figure 10. Monthly average surface NO_2 grouped into six regions as obtained from the OpenAQ database (black) and simulated by GEOS-CF (green). Vertical bars represent the standard deviation of hourly variability across all sites. Number of sites is given in the inset. Y-axis ranges vary by region.

4.4. Carbon Monoxide

Our analysis of simulated CO shows that the model has no significant global CO bias compared against satellite and surface observations. Figure 11 shows the global distribution and seasonal cycle of total column CO retrieved from MOPITT and derived from GEOS-CF. Local MOPITT averaging kernels were applied to the GEOS-CF CO profiles to obtain the column values. The model simulated CO pattern is in good agreement with MOPITT, with local maxima over major polluted areas (East China, India) and over biomass burning regions (South America and Central Africa). Similar to NO_2, the simulated CO columns over China are larger than the observations, possibly due to an overestimation of CO emissions over that region. The baseline anthropogenic CO emissions in GEOS-CF are scaled based on ODIAC emission trends, with strongest increases over China and India (Oda et al., 2018). Our scaling methodology assumes a constant CO/CO_2 emissions ratio, and any decrease in the CO/CO_2 emission ratio, e.g. due to a technology shift, would result in an overestimation of CO emissions.

The seasonal cycle of CO is determined by its shorter chemical lifetime during summer due to increased photochemical activity, which is reflected in lower NH concentrations during July and August where the model underestimates the MOPITT concentrations in the NH middle and high latitudes by 10-20% (Figure 11c). This underestimation is driven by a stronger than observed decrease of simulated total column CO during summertime, a pattern that is confirmed by comparisons against the GAW surface observations (Figure 12). While the model underestimates summertime surface CO in the NH, the opposite is true for the SH where model simulated concentrations during summer are higher than the observations. A low bias in CO is a long-standing issue in atmospheric chemistry models, commonly attributed to an underestimation of direct emissions and inconsistencies in the simulated distribution of the hydroxyl radical OH, the main atmospheric oxidant (Shindell et al., 2006; Strode et al., 2015, Flemming et al., 2015; Monks et al., 2015; Gaubert et al., 2016). The air mass-weighted mean

tropospheric OH in GEOS-CF is 11.9 x 10^5 molecules cm^{-3}, in good agreement with other models as well as estimates derived from methyl chloroform observations (Spivakovsky et al., 2000; Montzka et al., 2000; Naik et al., 2013). The inter-hemispheric (NH/SH) ratio is 1.33, again in good agreement with other model estimates (Naik et al., 2013) but higher than observation-derived values of 0.8-1.0 (Montzka et al., 2000; Prinn et al. 2001; Krol and Lelieveld 2003; Patra et al., 2014). This is consistent with an underestimation of summertime CO in the northern high-latitudes - as shown by the comparisons against MOPITT and the GAW surface observations (Figures 11 and 12) - and an overestimation of SH CO (Figure 12). An overestimation of NH OH in GEOS-CF is also supported by inversion studies using the GEOS-Chem CTM, which find that a similar OH correction is needed to match methane observations (Zhang et al., 2020).

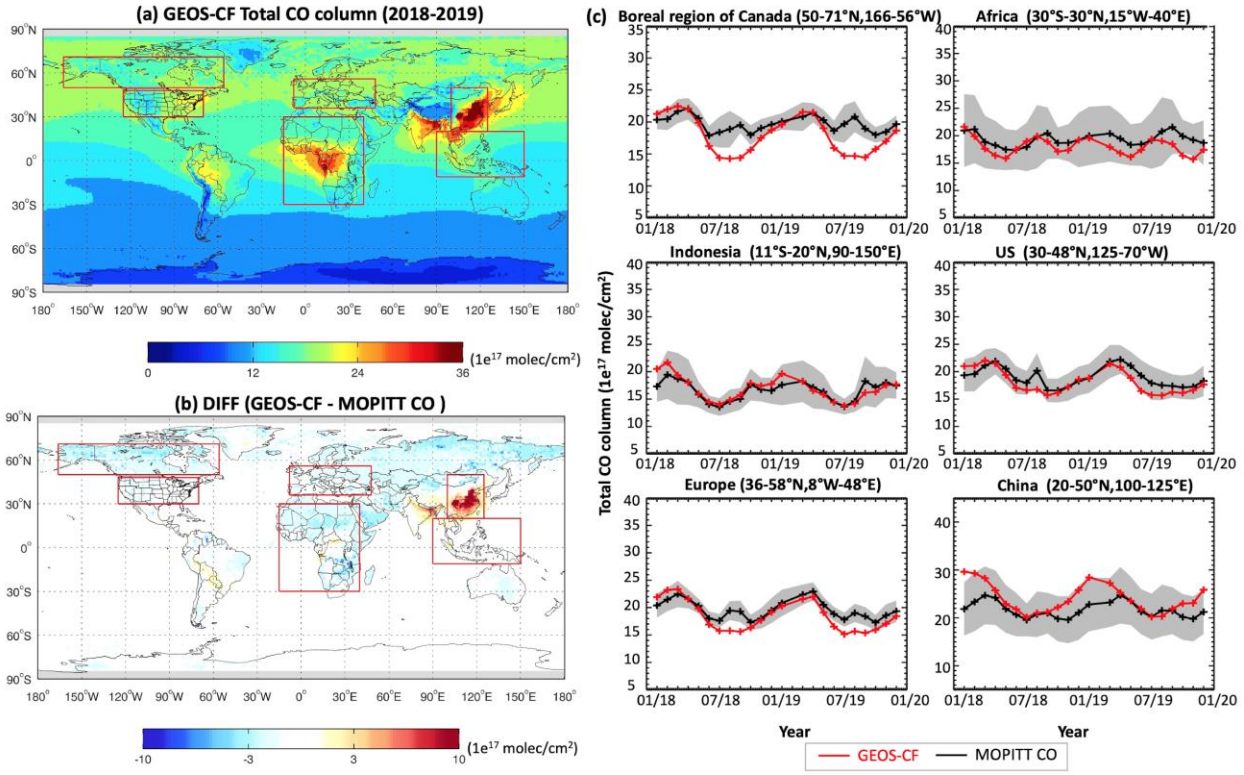

Figure 11. Comparison of GEOS-CF against MOPITT V8 total column CO. Top left panel shows the 2018-2019 average total CO column as simulated by GEOS-CF. Bottom left panel shows the difference between model simulated total column and MOPITT observations. Right panel shows the total CO time series averaged for six regions, as shown on the left.

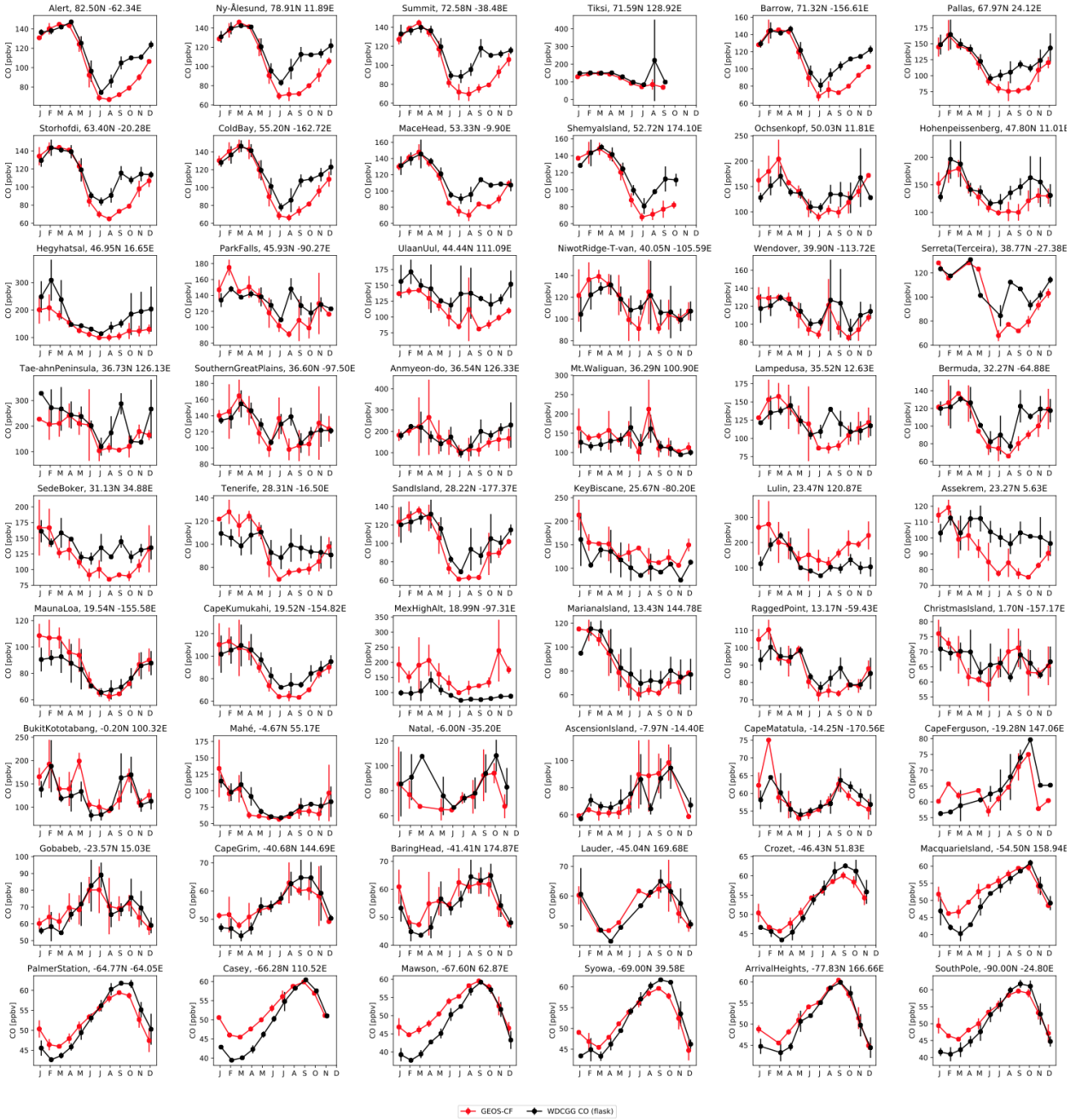

Figure 12. Monthly average surface CO as observed at 54 GAW sites (black) and simulated by GEOS-CF (red). Vertical bars represent the standard deviation of hourly variability. Y-axis ranges vary by station.

4.5. Aerosols

The evaluation of model simulated O_3, NO_2 and CO has shown that GEOS-CF reproduces many of the features of the tropospheric distribution of these trace gases. With respect to aerosols simulated by GEOS-Chem, our validation shows that GEOS-CF has a high bias but still captures many of the observed spatial and temporal patterns. A high bias in aerosols is a known issue in GEOS-Chem v12.0.1 used in GEOS-CF v1.0, and recent versions of GEOS-

Chem show improved simulation of aerosols including surface $PM_{2.5}$ (Luo et al., 2019; 2020; Carter et al., 2020).

Figure 13 compares model simulated AOD at 550nm against AERONET observations, and Figure 14 shows corresponding model-observation comparisons for surface $PM_{2.5}$. GEOS-CF overestimates the observations for both AOD and surface $PM_{2.5}$, pointing toward a systematic overestimation of aerosols in the model. On a relative basis, the overprediction is most pronounced for Europe and North America, and the largest absolute bias of surface $PM_{2.5}$ is found over Asia. We attribute part of the model overestimation to inadequate treatment of wet scavenging processes, which results in an overprediction of aerosol nitrate and ammonium, especially over Asia (Luo et al., 2019; 2020). Further, the QFED biomass burning emissions inventory uses enhancement factors based on the GOCART model to better match MODIS-observed AOD (Darmenov and Da Silva, 2015), which results in an overestimation of biomass burning emissions if the differences between the GEOS-Chem and GOCART aerosol parameterizations are not accounted for (Carter et al., 2020).

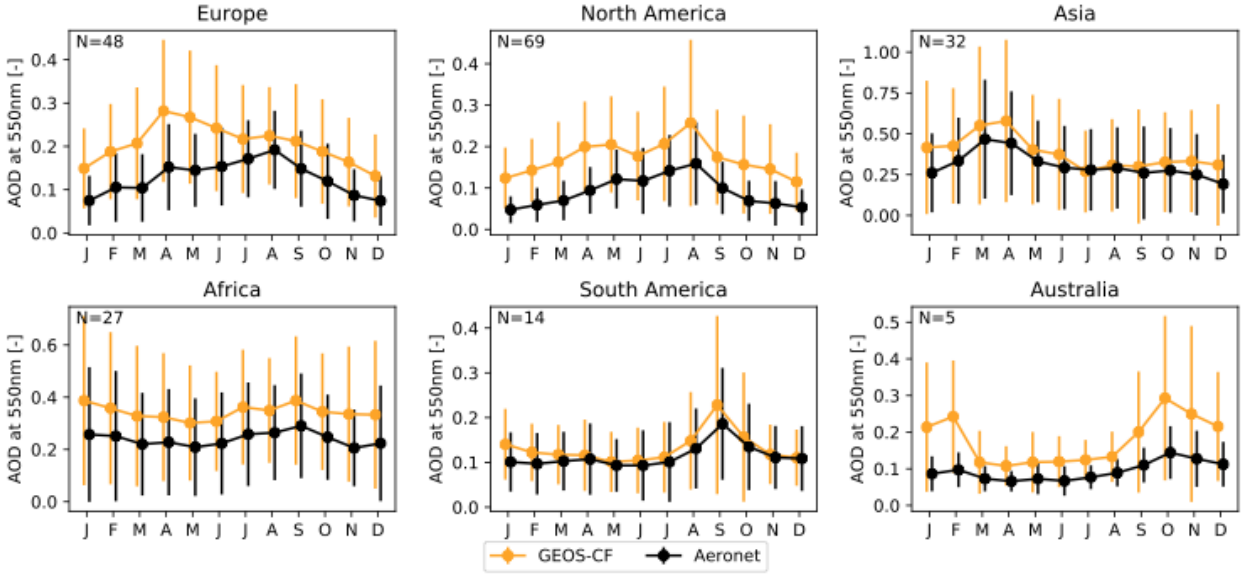

Figure 13. Monthly average Aerosol optical depth (AOD) at 550nm grouped into six regions as observed at AERONET sites (black) and simulated by GEOS-CF (orange). Vertical bars represent the standard deviation of daily variability. Number of sites is given in the inset. Y-axis ranges vary by region.

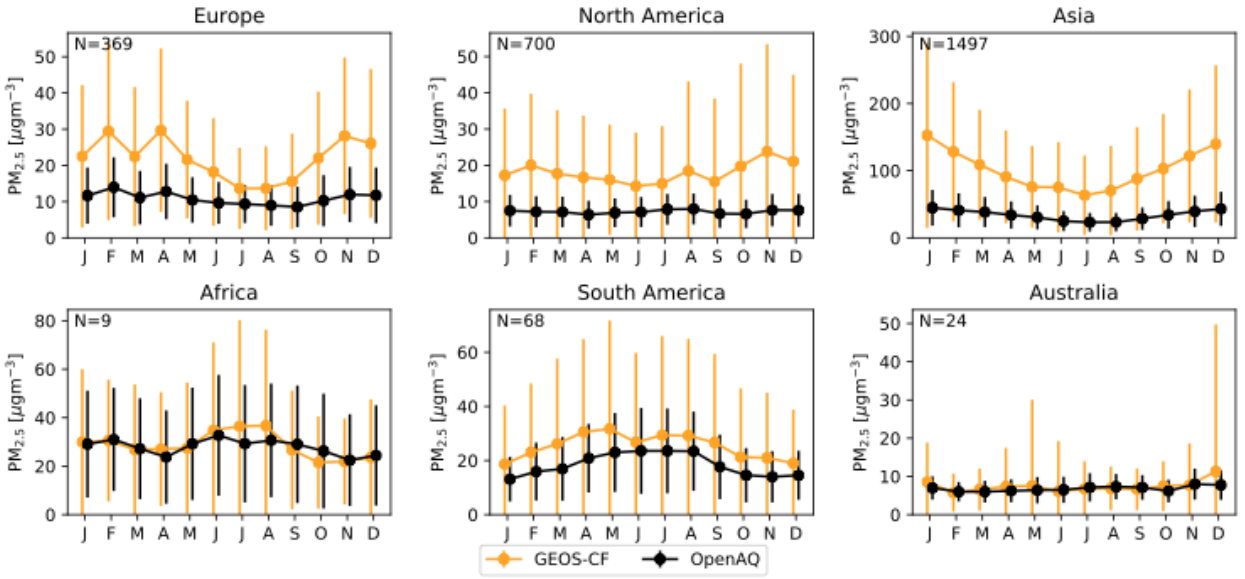

Figure 14: Monthly average surface $PM_{2.5}$ grouped into six regions as obtained from the OpenAQ database (black) and simulated by GEOS-CF (orange). Vertical bars represent the standard deviation of hourly variability. Number of sites is given in the inset. Y-axis ranges vary by region.

5 Evaluation of Model Forecasts

5.1. Comparison of Model Forecasts against Observations

GEOS-CF v1.0 does not directly assimilate trace gas observations and differences between the 1-day analysis and the model forecasts are thus mainly driven by variations between the forecasted and analyzed meteorological state. The meteorology not only impacts the flow of the constituents but also affects deposition and dynamically calculated emissions, including lightning NO_x, biogenic VOCs, sea salt aerosols, and dust (see Table 1). Further, the model forecasts assume persistence in the biomass burning emissions, meaning the fires observed during the analysis are assumed to continue burning and emitting the same amount for the next five days. The model thus does not capture changes in occurrence or intensity of wildfires, both of which can lead to significant changes in surface air pollution close to and downwind from the fires.

Figure 15 shows model-observation skill scores for the model analysis (forecast day -1) and the 5-day forecasts (forecast days +1 to +5) for O_3, NO_2, and $PM_{2.5}$. The results for the analysis are the same as discussed in Section 4 (Figure 3). Skill scores were calculated at each observation site individually before aggregating them in the form of boxplots, as shown in Figure 15. For all three evaluated species, the model analysis showed the best agreement with the observations. The median NMB of the model analysis is -0.01 for O_3, -0.26 for NO_2, and 1.50 for $PM_{2.5}$, with almost no difference between the analysis and the model forecasts. Relative to the analysis, the forecasted NRMSE and R become incrementally worse for the 1-day to 3-day lead forecasts, while there is little further deterioration between the 3-day forecasts and the 5-day forecasts. The median NRMSE is 0.36 for O_3, 0.42 for NO_2 and 1.05 for $PM_{2.5}$. The NRMSE slightly deteriorates with increasing forecast lead time, resulting in NRMSE's for the 5-day forecast of 0.4 for O_3, 0.45 for NO_2 and 1.07 for $PM_{2.5}$. This indicates that errors in the

meteorological forecasts (and biomass burning emissions) indeed impact the quality of the surface air quality forecasts. The increase in NRMSE is most pronounced for O_3, whose chemistry is strongly controlled by meteorological factors such as solar radiation, temperature, and humidity (e.g., Jacob et al., 1993; Sillman and Samson, 1995, Tarasova and Karpetchko, 2003). The largest change in skill score between analysis and forecasts is found for R, which drops from 0.6 for the analysis to 0.44 for the 5-day forecast for O_3, 0.32 to 0.15 for NO_2, and 0.47 to 0.17 for $PM_{2.5}$. Of the three analyzed skill scores, R is most sensitive to errors in the temporal pattern and we attribute a large fraction in the deterioration in R to transport errors in the forecasts, such as the evolution of frontal systems or the dispersion of smoke plumes. $PM_{2.5}$ is particularly sensitive to these factors given its large spatiotemporal gradients, comparatively long atmospheric lifetime, and strong sensitivity to changes in biomass burning emissions.

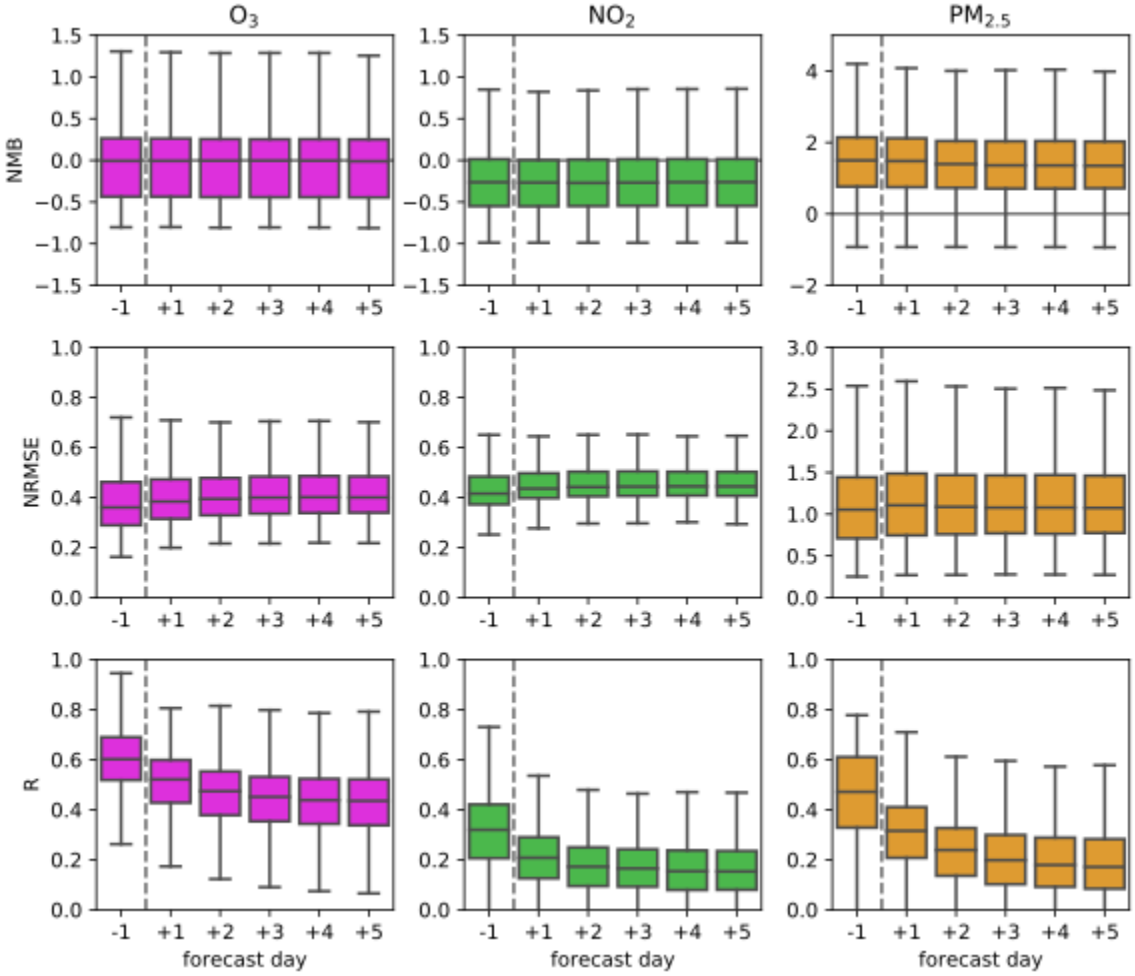

Figure 15. GEOS-CF model skill scores for the analysis (forecast day -1) and the 5-day forecasts (forecast day +1 to +5) relative to surface observations. Boxplots show the variation in the NMB, NRMSE, and R across all surface sites for O_3, NO_2, and $PM_{2.5}$.

5.2. Bias-corrected Local Forecasts

As discussed above, model-predicted concentrations of O_3, NO_2 and $PM_{2.5}$ can differ from the observations for a number of reasons, including model representation errors, uncertainties in the meteorology, or model biases arising from errors in the model treatment of

emissions, deposition, or atmospheric chemistry. One approach to deal with these issues is to quantify and correct these systematic model errors in a post-processing step. Such bias correction methods can be applied to near real-time model forecasts and have been found to be an effective tool to significantly improve local model predictions, e.g., by using mean subtraction (McKeen et al., 2005; Wilczak et al., 2006), historical analogs (Hamill and Whitaker, 2006), Kalman-filtering (Delle Monache et al., 2006; Djalalova et al., 2015), or kriging (Honoré et al., 2008). More recently, machine learning (ML) approaches have become popular to relate model output to air quality observations (e.g., Grange et al., 2018; Grange and Carslaw, 2019; Ivatt and Evans, 2020; Petetin et al., 2020). As discussed in Keller et al. (2020), bias-correction using ML can significantly reduce GEOS-CF model biases compared to surface observations. This is illustrated in Figure 16, which shows the GEOS-CF model skill scores for the same data set analyzed in Section 8 but using bias-corrected model concentrations instead of the original model output. The bias correction methodology is described in detail in Keller et al. (2020). It uses the XGBoost algorithm (Chen and Guestrin, 2016) to correct the original model predictions of O_3, NO_2, and $PM_{2.5}$ based on local meteorology and composition, as predicted by the GEOS-CF model. The ML algorithm was trained on analysis data for year 2018 and the results shown in Figure 16 are for year 2019.

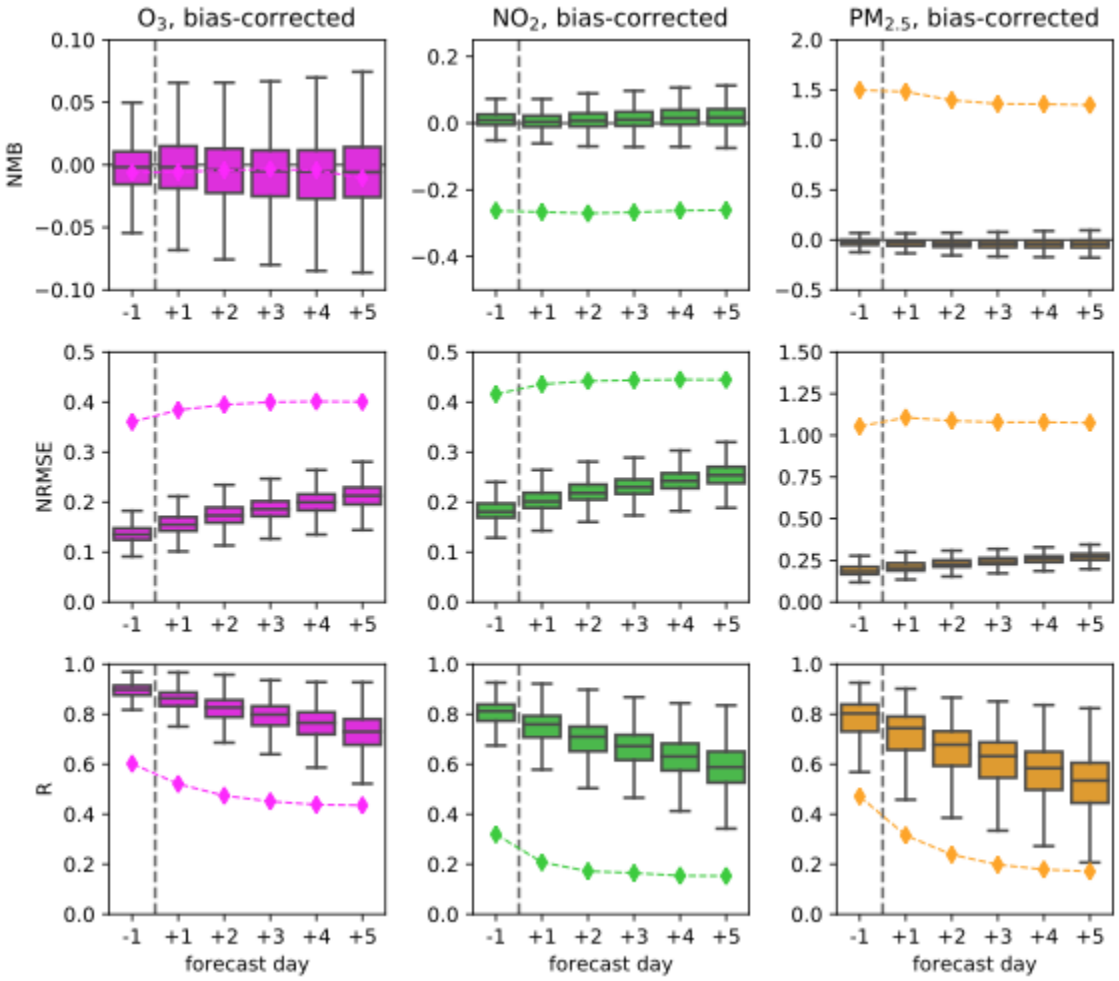

Figure 16. Similar to Figure 14 but boxplots indicate the GEOS-CF model skill scores for the bias-corrected analysis (forecast day -1) and the bias-corrected 5-day forecasts (forecast day +1

to +5) relative to surface observations as boxplots and the median statistics of the non-corrected model values from Figure 15 shown as diamonds.

Compared to the uncorrected model output (indicated by the diamonds in Figure 16), the bias-corrected model values agree much better with the observations for all species, skill scores, and lead times. For all three species, the NMB of the bias-corrected values is close to zero for both the analysis and the 5-day forecasts. This result is not unexpected given that the ML algorithm is designed to minimize the model bias. The NRMSE and R scores are also significantly improved compared to the original data, with RMSE values of 0.1-0.2 and R values between 0.6-0.9 for the analysis. The skill scores of the bias-corrected forecasts deteriorate more rapidly than is the case for the uncorrected output but still outperform the original forecasts for all five lead days. Since the ML algorithm was only trained on the analysis data, model errors in the meteorology forecasts will also negatively impact the quality of the bias correction applied to the (forecast) baseline, which explains the steady decline in the skill scores for the bias-corrected forecasts.

6 Conclusions

The GEOS-CF system provides global, near real-time and 5-day forecast simulations of atmospheric composition and meteorology at the high global resolution of 0.25 degrees -- including 5-day forecasts -- based on the GEOS-Chem chemistry module online within the GEOS GCM. Comparisons against a suite of satellite, ozonesonde and surface observations demonstrate that the model realistically captures the global distribution of a wide range of air constituents, including O_3, NO_2, and CO. For these three species, the model shows little biases at background locations, with NMB values ranging between -0.1 to +0.1. Like other atmospheric chemistry models, the model overestimates surface ozone in the NH during summer, especially over the south eastern US (Emmons et al., 2020, Fleming et al., 2015, Travis et al., 2016). While the horizontal resolution of 0.25 degrees is one of the highest for a global atmospheric chemistry forecast model, it is still not fine enough to resolve some of the meso-scale features of urban air pollution, which can lead to substantial model-observation mismatches when compared against urban air quality observations. Applying a bias-correction algorithm to the gridded model output, based on ML using historical observation-model comparisons, can lead to significant improvements of the model predictions over urban areas. This procedure, which can be automated as a post-processing step, offers an interesting option to provide highly localized forecasts at selected locations.

The GEOS-CF modeling system leverages components developed by the GEOS and the GEOS-Chem modeling communities and directly benefits from the continuous advancements provided by these groups. The current version of GEOS-CF (v1.0) incorporates GEOS-Chem v12.0.1. Several important updates have been added to GEOS-Chem since, and those will be included in future versions of GEOS-CF. This includes updates to the chemistry of isoprene (Bates and Jacob, 2019) and halogens (Wang et al., 2019), improved wet scavenging of aerosols (Luo et al., 2019; 2020), and updated ozone deposition over seawater (Pound et al., 2020). When implemented in future versions of GEOS-CF, these updates are expected to reduce the high bias observed in $PM_{2.5}$ and AOD as well as the high bias in surface ozone over the southern hemisphere.

Another model development focus will center around the assimilation of satellite observations of atmospheric constituents, which has been shown to lead to improved representation of atmospheric composition, in particular for longer-lived species such as O_3 and CO (Flemming et al., 2015). In its current form, GEOS-CF does not directly assimilate tropospheric trace gas observations, and the variability in constituent distribution is thus driven by the anthropogenic emission inventories, real-time biomass burning information, and the current meteorological state and its impact on dynamic emission sources such as biogenic emissions or sea salt aerosols. It should be noted that the anthropogenic emission inventories do not incorporate short-term, real-time changes in emissions, e.g., due to reduced human activities in the wake of the COVID-19 pandemic, and GEOS-CF v1.0 thus represents a business-as-usual estimate of the atmosphere (Keller et al., 2020). The inclusion of near real-time information for dynamic emission adjustment, e.g., based on traffic data or satellite observations, will be another model development focus.

GEOS-CF offers a new tool for academic researchers, air quality managers, and the public. Applications include flight campaign planning, support of satellite and other remote-sensing observations, interpretation of field campaign data (Dacic et al., 2020), and air quality research (Keller et al., 2020).

Acknowledgements

Resources supporting the model simulations were provided by the NASA Center for Climate Simulation at the Goddard Space Flight Center (https://www.nccs.nasa.gov/services/discover). CAK, KEK, DJJ, EWL, and SP acknowledge support by the NASA Modeling, Analysis and Prediction (MAP) Program.

Data Availability Statement

All model output is centrally stored at the NASA Center for Climate Simulation (NCCS). Public access to these archives is provided by the GMAO at https://gmao.gsfc.nasa.gov/weather_prediction/GEOS-CF/data_access/ in the form of weather maps and through model output access tools, including OPeNDAP and Hypertext Transfer Protocol (HTTP).

References

Amos, H. M., D. J. Jacob, C. D. Holmes, J. A. Fisher, Q. Wang, R. M. Yantosca, E. S. Corbitt, E. Galarneau, A. P. Rutter, M. S. Gustin, A. Steffen, J. J. Schauer, J. A. Graydon, V. L. St. Louis, R. W. Talbot, E. S. Edgerton, Y. Zhang, and E. M. Sunderland (2012), Gas-Particle Partitioning of Atmospheric Hg(II) and Its Effect on Global Mercury Deposition, *Atmos. Chem. Phys.*,12,591-603.

Bacmeister, J. T., Suarez, M. J., & Robertson, F. R. (2006). Rain reevaporation, boundary layer convection interactions, and Pacific rainfall patterns in a AGCM. *Journal of the Atmospheric Sciences*, 63, 3383–3403. https://doi.org/10.1175/JAS3791.1

Bates, K.H., and D.J. Jacob (2019), A new model mechanism for atmospheric oxidation of isoprene: global effects on oxidants, nitrogen oxides, organic products, and secondary organic aerosol, *Atmos. Chem. Phys*., 19, 9613-9640.

Bey, I., Jacob, D.J., Yantosca, R.M., Logan, J.A., Field, B.D., Fiore, A.M., Li, Q., Liu, H.Y., Mickley, L.J., Schultz, M.G. (2001), Global modeling of tropospheric chemistry with assimilated

meteorology: Model description and evaluation. *J. Geophys. Res. Atmospheres* 106, 23073–23095. https://doi.org/10.1029/2001JD000807

Bhattacharjee, P. S., Wang, J., Lu, C.-H., and Tallapragada, V. (2018), The implementation of NEMS GFS Aerosol Component (NGAC) Version 2.0 for global multispecies forecasting at NOAA/NCEP – Part 2: Evaluation of aerosol optical thickness, *Geosci. Model Dev.*, 11, 2333–2351, https://doi.org/10.5194/gmd-11-2333-2018.

Bian, H., Prather, M.J. (2002), Fast-J2: Accurate Simulation of Stratospheric Photolysis in Global Chemical Models. *J. Atmospheric Chem.* 41, 281–296. https://doi.org/10.1023/A:1014980619462

Borovikov, A., Cullather, R., Kovach, R. et al. (2019), GEOS-5 seasonal forecast system. *Clim Dyn 53*, 7335–7361. https://doi.org/10.1007/s00382-017-3835-2

Buchard, V., Randles, C.A., Silva, A.M. da, Darmenov, A., Colarco, P.R., Govindaraju, R., Ferrare, R., Hair, J., Beyersdorf, A.J., Ziemba, L.D., Yu, H., (2017), The MERRA-2 Aerosol Reanalysis, 1980 Onward. Part II: Evaluation and Case Studies. *J. Clim. 30*, 6851–6872.

Carn, S., (2019), Multi-Satellite Volcanic Sulfur Dioxide L4 Long-Term Global Database V3. https://doi.org/10.5067/measures/so2/data404

Carter, T. S., Heald, C. L., Jimenez, J. L., Campuzano-Jost, P., Kondo, Y., Moteki, N., Schwarz, J. P., Wiedinmyer, C., Darmenov, A. S., da Silva, A. M., and Kaiser, J. W. (2020), How emissions uncertainty influences the distribution and radiative impacts of smoke from fires in North America, *Atmos. Chem. Phys.*, 20, 2073–2097, https://doi.org/10.5194/acp-20-2073-2020.

Chen, T. and C. Guestrin (2016), XGBoost: A Scalable Tree Boosting System, *CoRR*, abs/1603.02754, 785–794, https://doi.org/10.1145/2939672.2939785.

Chou, M.-D. (1990). Parameterizations for the absorption of solar radiation by O_2 and CO_2 with applications to climate studies. *Journal of Climate*,3, 209–217.

Chou, M.-D. (1992). A solar radiation model for use in climate studies. *Journal of the Atmospheric Sciences*, 49, 762–772.

Chou, M.-D., & Suarez, M. J. (1994). An efficient thermal infrared radiation parameterization for use in general circulation models. *NASA Tech.Memorandum*, NASA/TM-1994–104606, Vol. 3, 85 p.. Greenbelt, MD: NASA Goddard Space Flight Center.

Colarco, P., da Silva, A., Chin, M., Diehl, T. (2010). Online simulations of global aerosol distributions in the NASA GEOS-4 model and comparisons to satellite and ground-based aerosol optical depth. *J. Geophys. Res. Atmospheres* 115, D14207, https://doi.org/10.1029/2009JD012820.

Croft, B., Wentworth, G., Martin, R. et al. (2016), Contribution of Arctic seabird-colony ammonia to atmospheric particles and cloud-albedo radiative effect. *Nat Commun* 7, 13444. https://doi.org/10.1038/ncomms13444

Dacic, N., John T. Sullivan, K. Emma Knowland, Glenn M. Wolfe, Luke D. Oman, Timothy A. Berkoff, Guillaume P. Gronoff (2020), Evaluation of NASA's high-resolution global composition simulations: Understanding a pollution event in the Chesapeake Bay during the summer 2017 OWLETS campaign, *Atmospheric Environment*, Volume 222, 117133, ISSN 1352-2310, https://doi.org/10.1016/j.atmosenv.2019.117133.

Darmenov, A.S., da Silva, A. (2015). The Quick Fire Emissions Dataset (QFED)—Documentation of versions 2.1, 2.2 and 2.4. *Technical Report Series on Global Modeling and Data Assimilation*. NASA//TM-2015-104606, Vol. 38, 212 pp.

Deeter, M. N., Edwards, D. P., Francis, G. L., Gille, J. C., Mao, D., Martinez-Alonso, S., Worden, H. M., Ziskin, D., and Andreae, M. O. (2019), Radiance-based retrieval bias mitigation for the MOPITT instrument: the version 8 product, *Atmospheric Measurement Techniques*, 12, 4561-4580, 10.5194/amt-12-4561-2019.

Delle Monache, L., T. Nipen, X. Deng, Y. Zhou, and R. Stull (2006), Ozone ensemble forecasts: 2. A Kalman filter predictor bias correction, *J. Geophys. Res.*, 111, p. D05308, 10.1029/2005JD006311

Delle Monache, L., Wilczak, J., Mckeen, S., Grell, G., Pagowski, M., Peckham, S., Stull, R., Mchenry, J. & Mcqueen, J. (2008) A Kalman-filter bias correction method applied to deterministic, ensemble averaged and probabilistic forecasts of surface ozone, *Tellus B: Chemical and Physical Meteorology*, 60:2, 238-249, DOI: 10.1111/j.1600-0889.2007.00332.x

Djalalova, I., Delle Monache, L., and Wilczak J. (2015), PM2.5 analog forecast and Kalman filter post-processing for the Community Multiscale Air Quality (CMAQ) model, *Atmospheric Environment*, Volume 108, Pages 76-87, ISSN 1352-2310, https://doi.org/10.1016/j.atmosenv.2015.02.021.

Dlugokencky, E. J., L. P. Steele, P. M. Lang, and K. A. Masarie (1994), The growth rate and distribution of atmospheric methane, *J. Geophys. Res*., 99, 17,021– 17,043, doi:10.1029/94JD01245.

Douglass, A. R., Stolarski, R. S., Strahan, S. E., & Connell, P. S. (2004). Radicals and reservoirs in the GMI chemistry and transport model: Comparison to measurements. *Journal of Geophysical Research*, 109, D16302. https://doi.org/10.1029/2004JD004632

Douglass, A. R., Strahan, S. E., Oman, L. D., & Stolarski, R. S. (2014). Understanding differences in chemistry climate model projections of stratospheric ozone. *Journal of Geophysical Research: Atmospheres*, 119, 4922–4939. https://doi.org/10.1002/2013JD021159

Duncan, B. N., Logan, J. A., Bey, I., Megretskaia, I. A., Yantosca, R. M., Novelli, P. C., Rinsland, C. P. (2007). The global budget of CO, 1988– 1997: Source estimates and validation with a global model. *Journal of Geophysical Research*, 112, D22301. https://doi.org/10.1029/2007JD008459

Duncan, B. N. , L. N. Lamsal, A. M. Thompson, Y. Yoshida, Z. Lu, D. G. Streets, M. M. Hurwitz, and K. E. Pickering (2016), A space-based, high-resolution view of notable changes in urban NOx pollution around the world (2005–2014). *J. Geophys. Res.* 121, 976–996.

Eastham, S.D., Weisenstein, D.K., Barrett, S.R.H., (2014), Development and evaluation of the unified tropospheric–stratospheric chemistry extension (UCX) for the global chemistry- 34 transport model GEOS-Chem. *Atmos. Environ.* 89, 52–63.

Emmons, L. K., Schwantes, R. H., Orlando, J. J., Tyndall, G., Kinnison, D., Lamarque, J.-F., et al. (2020). The Chemistry Mechanism in the Community Earth System Model version 2 (CESM2). *Journal of Advances in Modeling Earth Systems*, 12, e2019MS001882. https://doi.org/10.1029/2019MS001882

Evans, M. J., and Jacob, D. (2005). Impact of new laboratory studies of N_2O_5 hydrolysis on global model budgets of tropospheric nitrogen oxides, ozone, and OH, *Geophys. Res. Lett.*, 32, http://doi/.org/10.1029/2005gl022469

Eyring, V., T. G. Shepherd, & D. W. Waugh (Eds.) (2010). SPARC report on the evaluation of chemistry-climate models (SPARC Rep. 5, WCRP-132, WMO/TD 1526). Retrieved from http://www.atmosp.physics.utoronto.ca/SPARC/ccmval_final

Frith, S. M., N. A. Kramarova, R. S. Stolarski, R. D. McPeters, P. K. Bhartia, and G. J. Labow (2014), Recent changes in total column ozone based on the SBUV Version 8.6 Merged Ozone Data Set, *J. Geophys. Res. Atmos.*, 119, 9735–9751, doi:10.1002/2014JD021889.

Flemming, J., Huijnen, V., Arteta, J., Bechtold, P., Beljaars, A., Blechschmidt, A.-M., Diamantakis, M., Engelen, R. J., Gaudel, A., Inness, A., Jones, L., Josse, B., Katragkou, E., Marecal, V., Peuch, V.-H., Richter, A., Schultz, M. G., Stein, O., and Tsikerdekis, A. (2015). Tropospheric chemistry in the Integrated Forecasting System of ECMWF, *Geosci. Model Dev.*, 8, 975–1003, https://doi.org/10.5194/gmd-8-975-2015.

Fountoukis, C., Nenes, A. (2007). ISORROPIA II: a computationally efficient thermodynamic equilibrium model for K+–Ca2+–Mg2+–NH4 +–Na+–SO4 2 –NO3 - –Cl- –H2O aerosols. *Atmospheric Chem. Phys.* 7, 4639–4659

Garcia, R. R., & Boville, B. A. (1994). Downward control of the mean meridional circulation and temperature distribution of the polar winter stratosphere. *Journal of the Atmospheric Sciences*, 51, 2238–2245.

Gaubert, B., et al. (2016), Toward a chemical reanalysis in a coupled chemistry-climate model: An evaluation of MOPITT CO assimilation and its impact on tropospheric composition, *J. Geophys. Res. Atmos.*, 121, 7310–7343, doi:10.1002/2016JD024863.

Gelaro, R., McCarty, W., Suárez, M. J., Todling, R., Molod, A., Takacs, L., Randles, C. A., Darmenov, A., Bosilovich, M. G., Reichle, R., Wargan, K., Coy, L., Cullather, R., Draper, C., Akella, S., Buchard, V., Conaty, A., da Silva, A. M., Gu, W., Kim, G.- K., Koster, R., Lucchesi, R., Merkova, D., Nielsen, J. E., Partyka, G., Pawson, S., Putman, W., Rienecker, M., Schubert, S. D., Sienkiewicz, M., and Zhao, B. (2017). The Modern-Era Retrospective Analysis for Research and Applications, Version 2 (MERRA-2), *J. Climate*, 30, 5419–5454, https://doi.org/10.1175/JCLI-D-16- 0758.1.

Giles, D. M., Sinyuk, A., Sorokin, M. G., Schafer, J. S., Smirnov, A., Slutsker, I., et al. (2019). Advancements in the Aerosol Robotic Network (AERONET) Version 3 database—Automated near-real-time quality control algorithm with improved cloud screening for Sun photometer aerosol optical depth (AOD) measurements. *Atmospheric Measurement Techniques*, 12, 169–209. https://doi.org/10.5194/amt-12- 169-2019

Grange, S. K., Carslaw, D. C., Lewis, A. C., Boleti, E., and C. Hueglin (2018). Random forest meteorological normalisation models for Swiss PM 10 trend analysis, *Atmospheric Chemistry and Physics*, 18, 6223–6239, https://doi.org/10.5194/acp-18-6223-430.

Grange, S. K. and D. C. Carslaw (2019). Using meteorological normalisation to detect interventions in air quality time series, *Science of The Total Environment*, 653, 578–588, https://doi.org/10.1016/j.scitotenv.2018.10.344

Grosjean, D., and J. Harrison (1985), Response of chemiluminescence NOx analyzers and ultraviolet ozone analyzers to organic air pollutants, *Environ. Sci. Technol.*, 19, 862–865.

Hamill, T.M., J.S. Whitaker (2006), Probabilistic quantitative precipitation forecasts based on reforecast analogs: theory and application, *Mon. Weather Rev.*, 134, pp. 3209-3229, 10.1175/MWR3237.1

Helfand, H. M., & Schubert, S. D. (1995). Climatology of the simulated Great Plains low-level jet and its contribution to the continental moisture budget of the United States. *Journal of Climate*, 8, 784–806.

Hill, C., DeLuca, C., Balaji, V., Suarez, M., & da Silva, A. (2004). Architecture of the earth system modeling framework. *Computing in Science and Engineering*, 6(1), 18–28. https://doi.org/10.1109/MCISE.2004.1255817

Honoré, C., et al. (2008), Predictability of European air quality: Assessment of 3 years of operational forecasts and analyses by the PREV'AIR system, *J. Geophys. Res.*, 113, D04301, doi:10.1029/2007JD008761.

Hu, L., Jacob, D. J., Liu, X., Zhang, Y., Zhang, L., Kim, P. S., Sulprizio, M. P., and Yantosca, R. M. (2017). Global budget of tropospheric ozone: Evaluating recent model advances with satellite (OMI), aircraft (IAGOS), and ozonesonde observations, *Atmos. Environ.*, 167, 323–334, https://doi.org/10.1016/j.atmosenv.2017.08.036.

Hu, L., Keller, C. A., Long, M. S., Sherwen, T., Auer, B., Da Silva, A., Nielsen, J. E., Pawson, S., Thompson, M. A., Trayanov, A. L., Travis, K. R., Grange, S. K., Evans, M. J., and Jacob, D. J. (2018). Global simulation of tropospheric chemistry at 12.5 km resolution: performance and evaluation of the GEOS-Chem chemical module (v10-1) within the NASA GEOS Earth system model (GEOS-5 ESM), *Geosci. Model Dev.*, 11, 4603–4620, https://doi.org/10.5194/gmd-11-4603-2018.

Ivatt, P. D. and Evans, M. J. (2020). Improving the prediction of an atmospheric chemistry transport model using gradient-boosted regression trees, *Atmos. Chem. Phys.*, 20, 8063–8082, https://doi.org/10.5194/acp-20-8063-2020.

Jacob, D. J., J. A. Logan, G. M. Gardner, R. M. Yevich, C. M. Spivakovsky, S. C. Wofsy, S. Sillman, and M. J. Prather (1993), Factors regulating ozone over the United States and its export to the global atmosphere, *J. Geophys. Res.*, 98, 14,817–14,826, doi:10.1029/98JD01224.

Jaeglé, L., Quinn, P.K., Bates, T.S., Alexander, B., Lin, J.-T. (2011). Global distribution of sea salt aerosols: new constraints from in situ and remote sensing observations. *Atmospheric Chem. Phys.* 11, 3137–3157.

Jaeglé, L., Shah, V., Thornton, J. A., Lopez-Hilfiker, F. D., Lee, B. H., McDuffie, E. E., Fibiger, D., Brown, S. S., Veres, P., Sparks, T. L., Ebben, C. J., Wooldridge, P. J., Kenagy, H. S., Cohen, R. C., Weinheimer, A. J., Campos, T. L., Montzka, D. D., Digangi, J. P., Wolfe, G. M., Hanisco, T., Schroder, J. C., Campuzano-Jost, P., Day, D. A., Jimenez, J. L., Sullivan, A. P., Guo, H., and Weber, R. J. (2018). Nitrogen Oxides Emissions, Chemistry, Deposition, and Export Over the Northeast United States During the WINTER Aircraft Campaign, *J. Geophys. Res.-Atmos.*, 123, 12368-12393, https://doi.org/10.1029/2018JD029133.

Janssens-Maenhout, G., Crippa, M., Guizzardi, D., Dentener, F., Muntean, M., Pouliot, G., Keating, T., Zhang, Q., Kurokawa, J., Wankmüller, R., Denier van der Gon, H., Kuenen, J. J. P.,

Klimont, Z., Frost, G., Darras, S., Koffi, B., and Li, M. (2015). HTAP_v2.2: a mosaic of regional and global emission grid maps for 2008 and 2010 to study hemispheric transport of air pollution, *Atmos. Chem. Phys.*, 15, 11411–11432, https://doi.org/10.5194/acp-15-11411-2015.

Kang, D., R. Mathur, S.T. Rao, S. Yu (2008), Bias adjustment techniques for improving ozone air quality forecasts, *J. Geophys. Res.*, 113, p. D23308, 10.1029/2008JD010151

Keller, C.A., Long, M.S., Yantosca, R.M., Da Silva, A.M., Pawson, S., Jacob, D.J. (2014). HEMCO v1.0: a versatile, ESMF-compliant component for calculating emissions in atmospheric models. *Geosci. Model Dev.* 7, 1409–1417.

Keller, C. A., Evans, M. J., Knowland, K. E., Hasenkopf, C. A., Modekurty, S., Lucchesi, R. A., Oda, T., Franca, B. B., Mandarino, F. C., Díaz Suárez, M. V., Ryan, R. G., Fakes, L. H., and Pawson, S. (2020), Global Impact of COVID-19 Restrictions on the Surface Concentrations of Nitrogen Dioxide and Ozone, *Atmos. Chem. Phys. Discuss.*, https://doi.org/10.5194/acp-2020-685, in review.

Kleist D. T., D. F. Parrish, J. C. Derber, R. Treadon, W.-S. Wu, and S. Lord, (2009). Introduction of the GSI into the NCEPs Global Data Assimilation System. *Wea. Forecasting*, 24, 1691- 1705.

Krol, M. and Lelieveld, J. (2003). Can the variability in tropospheric OH be deduced from measurements of 1,1,1-trichloroethane (methyl chloroform)?, *J. Geophys. Res.*, 108, 4125, doi:10.1029/2002JD002423.

Lamsal, L. N., Krotkov, N. A., Vasilkov, A., Marchenko, S., Qin, W., Yang, E.-S., Fasnacht, Z., Joiner, J., Choi, S., Haffner, D., Swartz, W. H., Fisher, B., and Bucsela, E. (2020). OMI/Aura Nitrogen Dioxide Standard Product with Improved Surface and Cloud Treatments, *Atmos. Meas. Tech. Discuss.*, https://doi.org/10.5194/amt-2020-200, in review.

Lin, S. J. (2004). A vertically Lagrangian finite-volume dynamical core for global models. *Mon. Wea. Rev*., 132, 2293–2307.

Liu, H., Jacob, D. J., Bey, I., and Yantosca, R. M. (2001). Constraints from 210Pb and 7Be on wet deposition and transport in a global three-dimensional chemical tracer model driven by assimilated meteorological fields, *J. Geophys. Res.*, 106, 12109- 12128, http://doi/.org/10.1029/2000jd900839.

Liu, F., Choi, S., Li, C., Fioletov, V.E., McLinden, C.A., Joiner, J., Krotkov, N.A., Bian, H., Janssens-Maenhout, G., Darmenov, A.S., da Silva, A.M. (2018). A new global anthropogenic SO2 emission inventory for the last decade: a mosaic of satellite-derived and bottom-up emissions. *Atmospheric Chem. Phys.* 18, 16571–16586. https://doi.org/10.5194/acp-18-16571-2018

Lock, A. P., Brown, A. R., Bush, M. R., Martin, G. M., & Smith, R. N. B. (2000). A new boundary layer mixing scheme. Part I: Scheme description and single-column model tests. *Monthly Weather Review*, 138, 3187–3199.

Long, M. S., Yantosca, R., Nielsen, J. E., Keller, C. A., da Silva, A., Sulprizio, M. P., Pawson, S., and Jacob, D. J. (2015). Development of a grid-independent GEOS-Chem chemical transport model (v9-02) as an atmospheric chemistry module for Earth system models, *Geoscientific Model Development*, 8, 595-602, http://doi/.org/10.5194/gmd-8-595-2015

941 Louis, J., & Geleyn, J. (1982). A short history of the PBL parameterization at ECMWF. In
942 Proceedings of the ECMWF workshop on planetary boundary layer parameterization (pp. 59–
943 80). Reading, UK: ECMWF.

944 Lucchesi, R. (2015). File Specification for GEOS-5 FP-IT. GMAO Office Note No. 2 (Version
945 1.4) 58 pp, available from http://gmao.gsfc.nasa.gov/pubs/office_notes.php.

946 Luo, G., Yu, F., and Schwab, J. (2019). Revised treatment of wet scavenging processes
947 dramatically improves GEOS-Chem 12.0.0 simulations of surface nitric acid, nitrate, and
948 ammonium over the United States, *Geosci. Model Dev.*, 12, 3439–3447,
949 https://doi.org/10.5194/gmd-12-3439-2019.

950 Luo, G., F. Yu, and J. Moch (2020). Further improvement of wet process treatments in GEOS-
951 Chem v12.6.0: impact on global distributions of aerosols and aerosol precursors, *Geosci. Model*
952 *Dev.*, 13, 2879-2903.

953 Mao, J., Jacob, D.J., Evans, M.J., Olson, J.R., Ren, X., Brune, W.H., Clair, J.M.St., Crounse,
954 J.D., Spencer, K.M., Beaver, M.R., Wennberg, P.O., Cubison, M.J., Jimenez, J.L., Fried, A.,
955 Weibring, P., Walega, J.G., Hall, S.R., Weinheimer, A.J., Cohen, R.C., Chen, G., Crawford, J.H.,
956 McNaughton, C., Clarke, A.D., Jaeglé, L., Fisher, J.A., Yantosca, R.M., Le Sager, P., Carouge,
957 C. (2010). Chemistry of hydrogen oxide radicals (HOx) in the Arctic troposphere in spring.
958 *Atmospheric Chem. Phys*. 10, 5823–5838. https://doi.org/10.5194/acp-10-5823-2010

959 Mao, J., Paulot, F., Jacob, D.J., Cohen, R.C., Crounse, J.D., Wennberg, P.O., Keller, C.A.,
960 Hudman, R.C., Barkley, M.P., Horowitz, L.W. (2013). Ozone and organic nitrates over the
961 eastern United States: Sensitivity to isoprene chemistry. *J. Geophys. Res.* Atmospheres 118,
962 11,256–11,268.

963 Marais, E. A., Jacob, D. J., Jimenez, J. L., Campuzano-Jost, P., Day, D. A., Hu, W., Krechmer,
964 J., Zhu, L., Kim, P. S., Miller, C. C., Fisher, J. A., Travis, K., Yu, K., Hanisco, T. F., Wolfe, G.
965 M., Arkinson, H. L., Pye, H. O. T., Froyd, K. D., Liao, J., and McNeill, V. F. (2016). Aqueous-
966 phase mechanism for secondary organic aerosol formation from isoprene: application to the
967 southeast United States and co-benefit of SO2 emission controls, *Atmos. Chem. Phys.*, 16, 1603-
968 1618, http://doi/.org/10.5194/acp-16-1603-2016.

969 Marais, E. and C. Wiedinmyer (2016), Air quality impact of Diffuse and Inefficient Combustion
970 Emissions in Africa (DICE-Africa), *Environ. Sci. Technol.*, 50(19), 10739–10745,
971 doi:10.1021/acs.est.6b02602.

972 Marécal, V., et al. (2015). A regional air quality forecasting system over Europe: the MACC-II
973 daily ensemble production, *Geosci. Model Dev.*, 8, 2777–2813, https://doi.org/10.5194/gmd-8-
974 2777-2015.

975 Martin, R. V., Jacob, D. J., Yantosca, R. M., Chin, M., and Ginoux, P. (2003). Global and
976 regional decreases in tropospheric oxidants from photochemical effects of aerosols, *J. Geophys.*
977 *Res.*, 108, n/a-n/a, http://doi/.org/10.1029/2002jd002622.

978 McFarlane, N. A. (1987). The effect of orographically excited gravity-wave drag on the
979 circulation of the lower stratosphere and troposphere. *Journal of the Atmospheric Sciences*, 44,
980 1775–1800.

981 McKeen S., J. Wilczak, G. Grell, I. Djalalova, S. Peckham, E.-Y. Hsie, W. Gong, V. Bouchet, S.
982 Menard, R. Moffet, J. McHenry, J. McQueen, Y. Tang, G.R. Carmichael, M. Pagowski, A. Chan,

T. Dye, G. Frost, P. Lee, R. Mathur (2005), Assessment of an ensemble of seven real-time ozone forecasts over eastern North America during the summer of 2004, *J. Geophys. Res.*, 110, p. D21307, 10.1029/2005JD005858

Miller, C., Jacob, D. J., Marais, E. A., Yu, K., Travis, K. R., Kim, P. S., Fisher, J. A., Zhu, L., Wolfe, G. M., Hanisco, T. F., Keutsch, F. N., Kaiser, J., Min, K.-E., Brown, S. S., Washenfelder, R. A., González Abad, G., and Chance, K. (2017). Glyoxal yield from isoprene oxidation and relation to formaldehyde: chemical mechanism, constraints from SENEX aircraft observations, and interpretation of OMI satellite data, *Atmos. Chem. Phys.*, 17, 8725–8738, https://doi.org/10.5194/acp-17-8725-2017.

Molod, A., Takacs, L. L., Suarez, M. J., Bacmeister, J. T., Song, I.- S., and Eichmann, A. (2012). The GEOS-5 Atmospheric General Circulation Model: Mean Climate and Development from MERRA to Fortuna. NASA Tech. Memo. 104606, Vol. 28, Tech. Rep. Series on Global Modeling and Data Assimilation, edited by: Suarez, M. J., 117 pp.

Molod, A., Partyka, G., & Suarez, M. (2013). The impact of limiting ocean roughness on GEOS-5 AGCM tropical cyclone forecasts. *Geophysical Research Letters*, 40, 411–416. https://doi.org/10.1029/2012GL053979

Molod, A., Takacs, L., Suarez, M., and Bacmeister, J. (2015). Development of the GEOS-5 atmospheric general circulation model: evolution from MERRA to MERRA2, *Geosci. Model Dev.*, 8, 1339-1356, doi:10.5194/gmd-8-1339-2015.

Molod, A., E. Hackert, Y. Vikhliaev, B. Zhao, D. Barahona, G. Vernieres, A. Borovikov, R. M. Kovach, J. Marshak, S. Schubert, Z. Li, Y.-K. Lim, L. C. Andrews, R. Cullather, R. Koster, D. Achuthavarier, J. Carton, L. Coy, J. L. M. Freire, K. M. Longo, K. Nakada, and S. Pawson, (2020). GEOS-S2S Version 2: The GMAO High Resolution Coupled Model and Assimilation System for Seasonal Prediction. *J. Geophy. Res. - Atmos.*, 125, e2019JD031767. doi: 10.1029/2019JD031767.

Monks, S. A., Arnold, S. R., Emmons, L. K., Law, K. S., Turquety, S., Duncan, B. N., Flemming, J., Huijnen, V., Tilmes, S., Langner, J., Mao, J., Long, Y., Thomas, J. L., Steenrod, S. D., Raut, J. C., Wilson, C., Chipperfield, M. P., Diskin, G. S., Weinheimer, A., Schlager, H., and Ancellet, G. (2015). Multi-model study of chemical and physical controls on transport of anthropogenic and biomass burning pollution to the Arctic, *Atmos. Chem. Phys.*, 15, 3575–3603, doi:10.5194/acp-15-3575-2015.

Montzka, S. A., Spivakovsky, C. M., Butler, J. H., Elkins, J. W., Lock, L. T., and Mondeel, D. J. (2000). New observational constraints, for atmospheric hydroxyl on global and hemispheric scales, *Science*, 288, 500–503.

Moorthi, S., & Suarez, M. J. (1992). Relaxed Arakawa Schubert: A parameterization of moist convection for general circulation models. *Monthly Weather Review*, 120, 978–1002.

Murray, L. T., D. J. Jacob, J. A. Logan, R. C. Hudman, and W. J. Koshak (2012), Optimized regional and interannual variability of lightning in a global chemical transport model constrained by LIS/OTD satellite data, *J. Geophys. Res.*, 117, D20307, doi:10.1029/2012JD017934.

Naik, V., Voulgarakis, A., Fiore, A. M., Horowitz, L. W., Lamarque, J.-F., Lin, M., Prather, M. J., Young, P. J., Bergmann, D., Cameron-Smith, P. J., Cionni, I., Collins, W. J., Dalsøren, S. B., Doherty, R., Eyring, V., Faluvegi, G., Folberth, G. A., Josse, B., Lee, Y. H., MacKenzie, I. A.,

Nagashima, T., van Noije, T. P. C., Plummer, D. A., Righi, M., Rumbold, S. T., Skeie, R., Shindell, D. T., Stevenson, D. S., Strode, S., Sudo, K., Szopa, S., and Zeng, G. (2013). Preindustrial to present-day changes in tropospheric hydroxyl radical and methane lifetime from the Atmospheric Chemistry and Climate Model Intercomparison Project (ACCMIP), *Atmos. Chem. Phys.*, 13, 5277–5298, doi:10.5194/acp-13-5277-2013.

Nielsen, J. E., S. Pawson, A. Molod, B. Auer, A. M. da Silva, A. R. Douglass, B. N. Duncan, Q. Liang, M. E. Manyin, L. D. Oman, W. M. Putman, S. E. Strahan, and K. Wargan (2017). Chemical Mechanisms and their Applications in the Goddard Earth Observing System (GEOS) Earth System Model. *J. Adv. Model. Earth Syst.*, 9, 3019-3044. DOI: 10.1002/2017MS001011.

Oda, T., Maksyutov, S., and Andres, R. J. (2018). The Open-source Data Inventory for Anthropogenic CO2, version 2016 (ODIAC2016): a global monthly fossil fuel CO2 gridded emissions data product for tracer transport simulations and surface flux inversions, *Earth Syst. Sci. Data*, 10, 87–107, https://doi.org/10.5194/essd-10-87-2018.

Oman, L. D., & Douglass, A. R. (2014). Improvements in total column ozone in GEOSCCM and comparisons with a new ozone-depleting substances scenario. *Journal of Geophysical Research: Atmospheres*, 119, 5613–5624. https://doi.org/10.1002/2014JD021590

Orbe, C., L. D. Oman, S. E. Strahan, D. W. Waugh, L. L. Takacs, S. Pawson, and A. M. Molod (2017). Large-Scale Atmospheric Transport in GEOS Replay Simulations. *J. Adv. Model. Earth Sy*, 9, 7, 2545-2560. DOI: 10.1002/2017MS001053.

Park, R. J., Jacob, D. J., Chin, M., and Martin, R. V. (2003). Source of carbonaceous aerosols over the United States and implications for natural visibility, *J. Geophys. Res.*, 108, 4355, https://doi.org/10.1029/2002JD003190.

Park, R. J., Jacob, D. J., Field, B. D., Yantosca, R. M., and Chin, M. (2004). Natural and transboundary pollution influences on sulfate-nitrate-ammonium aerosols in the United States: Implications for policy, *J Geophys Res-Atmos*, 109, http://doi/.org/10.1029/2003jd004473

Parrella, J.P., Jacob, D.J., Liang, Q., Zhang, Y., Mickley, L.J., Miller, B., Evans, M.J., Yang, X., Pyle, J.A., Theys, N., Van Roozendael, M. (2012). Tropospheric bromine chemistry: implications for present and pre-industrial ozone and mercury. *Atmospheric Chem. Phys.* 12, 6723–6740. https://doi.org/10.5194/acp-12-6723-2012

Patra, P., Krol, M., Montzka, S., Arnold, T., Atlas, E. L., Lintner, B., Stephens, B., Xiang, B., Elkins, J., Fraser, P., et al. (2014). Observational evidence for interhemispheric hydroxyl-radical parity, *Nature*, 513, 219.

Pawson, S., Stajner, I., Kawa, S. R., Hayashi, H., Tan, W., Nielsen, J. E., . . . Livesey, N. J. (2007). Stratospheric transport using six-hour averaged winds from a data assimilation system. *Journal of Geophysical Research*, 112, D23103. https://doi.org/10.1029/2006JD007673

Petetin, H., Bowdalo, D., Soret, A., Guevara, M., Jorba, O., Serradell, K., and Pérez García-Pando, C. (2020). Meteorology-normalized impact of the COVID-19 lockdown upon NO2 pollution in Spain, *Atmos. Chem. Phys.*, 20, 11119–11141, https://doi.org/10.5194/acp-20-11119-2020.

Pound, R. J., Sherwen, T., Helmig, D., Carpenter, L. J., and Evans, M. J. (2020). Influences of oceanic ozone deposition on tropospheric photochemistry, *Atmos. Chem. Phys.*, 20, 4227–4239, https://doi.org/10.5194/acp-20-4227-2020.

Price, C., and D. Rind (1992), A simple lightning parameterization for calculating global lightning distributions, *J. Geophys. Res.*, 97, 9919–9933, doi:10.1029/92JD00719.

Price, C., and D. Rind (1993), What determines the cloud-to-ground lightning fraction in thunderstorms, *Geophys. Res. Lett.*, 20(6), 463–466, doi:10.1029/93GL00226.

Price, C., and D. Rind (1994), Modeling global lightning distributions in a general-circulation model, *Mon. Weather Rev.*, 122(8), 1930–1939, doi:10.1175/1520-0493(1994)122<1930:MGLDIA>2.0.CO;2

Prinn, R. G., Huang, J., Weiss, R. F., Cunnold, D. M., Fraser, P. J., Simmonds, P. G., McCulloch, A., Harth, C., Salameh, P., O'Doherty, S., Wang, R. H. J., Porter, L, and Miller, B. R. (2001). Evidence for substantial variations of atmospheric hydroxyl radicals over the past two decades, *Science*, 292, 1882–1888.

Putman, W. and Lin, S.-J. (2007). Finite Volume Transport on Various Cubed Sphere Grids. *J. Comput. Phys.*, 227, 55–78. doi:10.1016/j.jcp.2007.07.022.

Pye, H.O.T., Liao, H., Wu, S., Mickley, L.J., Jacob, D.J., Henze, D.K., Seinfeld, J.H. (2009). 36 Effect of changes in climate and emissions on future sulfate-nitrate-ammonium aerosol levels in the United States. *J. Geophys. Res. Atmospheres* 114, D01205. https://doi.org/10.1029/2008JD010701

Randles, C. A., and Coauthors (2017). The MERRA-2 aerosol reanalysis, 1980 onward, Part I: System description and data assimilation evaluation. *J. Climate*, 30, 6823–6850, doi:https://doi.org/10.1175/JCLI-D-16-0609.1

Ridley, D. A., Heald, C. L., and Ford, B. J. (2012). North African dust export and impacts: an integrated satellite and model perspective, *J. Geophys. Res.*, 117, D02202, https://doi.org/10.1029/2011JD016794.

Rienecker, M.M., M.J. Suarez, R. Todling, J. Bacmeister, L. Takacs, H.-C. Liu, W. Gu, M. Sienkiewicz, R.D. Koster, R. Gelaro, I. Stajner, and E. Nielsen (2008). The GEOS-5 Data Assimilation System - Documentation of Versions 5.0.1, 5.1.0, and 5.2.0. Technical Report Series on Global Modeling and Data Assimilation 104606, Vol. 27.

Rienecker and Coauthors (2011). MERRA - NASA's Modern-Era Retrospective Analysis for Research and Applications. *J. Climate*, 24, 3624-3648, doi:10.1175/JCLI-D-11-00015.1.

Rotman, D.A., Tannahill, J.R., Kinnison, D.E., Connell, P.S., Bergmann, D., Proctor, D., Rodriguez, J.M., Lin, S.J., Rood, R.B., Prather, M.J., Rasch, P.J., Considine, D.B., Ramaroson, R., Kawa, S.R. (2001). Global modeling initiative assessment model: model description, integration, and testing of the transport shell. *Journal of Geophysical Research* 106, 1669e1691.

Sandu, A., Sander, R. (2006). Technical note: Simulating chemical systems in Fortran90 and Matlab with the Kinetic PreProcessor KPP-2.1. *Atmospheric Chem. Phys.* 6, 187–195. https://doi.org/10.5194/acp-6-187-2006

Sherwen, T., Schmidt, J.A., Evans, M.J., Carpenter, L.J., Gro\s smann, K., Eastham, S.D., Jacob, D.J., Dix, B., Koenig, T.K., Sinreich, R., Ortega, I., Volkamer, R., Saiz-Lopez, A., Prados-Roman, C., Mahajan, A.S., Ordóñez, C. (2016). Global impacts of tropospheric halogens (Cl, Br, I) on oxidants and composition in GEOS-Chem. *Atmospheric Chem. Phys.* 16, 12239–12271.

Schumann, U., and H. Huntrieser (2007), The global lightning-induced nitrogen oxides source, *Atmos. Chem. Phys.*, 7(14), 3823–3907, doi:10.5194/acp-7-3823-2007.

Seinfeld, J.H. and S.N. Pandis (2016). Atmospheric Chemistry and Physics: From Air Pollution to Climate Change. John Wiley & Sons, Hoboken.

Shah, V., Jacob, D. J., Li, K., Silvern, R. F., Zhai, S., Liu, M., Lin, J., and Zhang, Q. (2020). Effect of changing NOx lifetime on the seasonality and long-term trends of satellite-observed tropospheric NO2 columns over China, *Atmos. Chem. Phys.*, 20, 1483–1495, https://doi.org/10.5194/acp-20-1483-2020.

Shindell, D. T., et al. (2006), Multimodel simulations of carbon monoxide: Comparison with observations and projected near-future changes, *J. Geophys. Res.*, 111, D19306, doi:10.1029/2006JD007100.

Sillman, S., and P. J. Samson (1995), Impact of temperature on oxidant photochemistry in urban, polluted rural and remote environments, *J. Geophys. Res.*, 100, 11,497–11,508, doi:10.1029/94JD02146.

Solomon, S., Portmann, R. W., Sasaki, T., Hofmann, D. J., and Thompson, D. W. J. (2005). Four decades of ozonesonde measurements over Antarctica, *Journal of Geophysical Research-Atmospheres*, 110, 10.1029/2005jd005917.

Spivakovsky, C. M., Logan, J. A., Montzka, S. A., Balkanski, Y. J., Foreman-Fowler, M., Jones, D. B. A., Horowitz, L. W., Fusco, A. C., Brenninkmeijer, C. A. M., Prather, M. J., Wofsy, S. C., and McElroy, M. B. (2000). Three-dimensional climatological distribution of tropospheric OH: Update and evaluation, *J. Geophys. Res.*, 105, 8931–8980.

Steinbacher, M., Zellweger, C., Schwarzenbach, B., Bugmann, S., Buchmann, B., Ordóñez, C., Prevot, A. S. H., and Hueglin, C. (2007), Nitrogen oxide measurements at rural sites in Switzerland: Bias of conventional measurement techniques, *J. Geophys. Res.*, 112, D11307, doi:10.1029/2006JD007971.

Streets, D.G., Canty T., Carmichael, G.R. , de Foy, B. Dickerson, R.R, Duncan, B.N., Edwards, D.P. , Haynes, J.A., Henze, D.K., Houyoux, M.R., Jacob, D.J., Krotkov, N.A., Lamsal, L.N., Liu, Y., Lu, Z., Martin, R.V., Pfister, G.G., Pinder, R.W., Salawitch, R.J., and K.J. Wecht (2013), Emissions estimation from satellite retrievals: A review of current capability, *Atmospheric Environment*, Volume 77, Pages 1011-1042, https://doi.org/10.1016/j.atmosenv.2013.05.051.

Strode, S. A., Duncan, B. N., Yegorova, E. A., Kouatchou, J., Ziemke, J. R., and Douglass, A. R. (2015). Implications of carbon monoxide bias for methane lifetime and atmospheric composition in chemistry climate models, *Atmos. Chem. Phys.*, 15, 11789–11805, https://doi.org/10.5194/acp-15-11789-2015.

Stettler, M., Eastham, S., and Barrett, S, (2011). Air quality and public health impacts of UK airports. Part I: Emissions, *Atmos. Environ.*, 45, 5415–5424, doi:10.1016/j.atmosenv.2011.07.012, 2011.

Strahan, S.E., B.N. Duncan and P. Hoor (2007). Observationally-derived diagnostics of transport in the lowermost stratosphere and their application to the GMI chemistry transport model , *Atmos. Chem. Phys.*, 7, 2435-2445.

Suarez, M., Trayanov, A., Hill, C., Schopf, P., & Vikhliaev, Y. (2007). MAPL: A high-level programming paradigm to support more rapid and robust encoding of hierarchical trees of interacting high-performance components. In Proceedings of the 2007 symposium on component and framework technology in high-performance and scientific computing (pp. 11–20). https://doi.org/10.1145/1297385.1297388

Tarasova, O. A., and A. Y. Karpetchko (2003), Accounting for local meteorological effects in the ozone time-series of Lovozero (Kola Peninsula), *Atmos. Chem. Phys.*, 3(4), 941–949, doi:10.5194/acp-3-941-2003.

Thompson, A. M., Witte, J. C., Sterling, C., Jordan, A., Johnson, B. J., Oltmans, S. J., Fujiwara, M., Vomel, H., Allaart, M., Piters, A., Coetzee, G. J. R., Posny, F., Corrales, E., Diaz, J. A., Felix, C., Komala, N., Lai, N., Nguyen, H. T. A., Maata, M., Mani, F., Zainal, Z., Ogino, S. Y., Paredes, F., Penha, T. L. B., da Silva, F. R., Sallons-Mitro, S., Selkirk, H. B., Schmidlin, F. J., Stubi, R., and Thiongo, K. (2017). First Reprocessing of Southern Hemisphere Additional Ozonesondes (SHADOZ) Ozone Profiles (1998-2016): 2. Comparisons With Satellites and Ground-Based Instruments, *Journal of Geophysical Research-Atmospheres*, 122, 13000-13025, 10.1002/2017jd027406.

Travis, K. R., Jacob, D. J., Fisher, J. A., Kim, P. S., Marais, E. A., Zhu, L., Yu, K., Miller, C. C., Yantosca, R. M., Sulprizio, M. P., Thompson, A. M., Wennberg, P. O., Crounse, J. D., St. Clair, J. M., Cohen, R. C., Laughner, J. L., Dibb, J. E., Hall, S. R., Ullmann, K., Wolfe, G. M., Pollack, I. B., Peischl, J., Neuman, J.A., and Zhou, X. (2016). Why do models overestimate surface ozone in the Southeast United States?, *Atmos. Chem. Phys.*, 16, 13561–13577, https://doi.org/10.5194/acp-16-13561-2016.

Travis, K. R. and Jacob, D. J. (2019). Systematic bias in evaluating chemical transport models with maximum daily 8 h average (MDA8) surface ozone for air quality applications: a case study with GEOS-Chem v9.02, *Geosci. Model Dev.*, 12, 3641–3648, https://doi.org/10.5194/gmd-12-3641-2019.

Wang, Q., Jacob, D.J., Spackman, J.R., Perring, A.E., Schwarz, J.P., Moteki, N., Marais, E.A., Ge, C., Wang, J., Barrett, S.R.H. (2014). Global budget and radiative forcing of black carbon aerosol: Constraints from pole-to-pole (HIPPO) observations across the Pacific. *J. Geophys. Res. Atmospheres* 119, 195–206.

Wang, X., D.J. Jacob, M.P. Sulprizio, S.D. Eastham, L. Zhu, Q. Chen, B. Alexander, T. Sherwen, M.J. Evans, B.H. Lee, J.D. Haskins, F.D. Lopez-Hilfike, J.A. Thornton, G.L. Huey, and H. Liao (2019), The role of chlorine in global tropospheric chemistry, *Atmos. Chem. Phys.*, 19, 3981-4003.

Wargan, K., S. Pawson, M. A. Olsen, J. C. Witte, A. R. Douglass, J. R. Ziemke, S. E. Strahan, and J. E. Nielsen (2015). The Global Structure of Upper Troposphere-Lower Stratosphere Ozone in GEOS-5: A Multi-Year Assimilation of EOS Aura Data. *J. Geophys. Res. - Atmos*, 120, 2013-2036. doi: 10.1002/2014JD022493.

Wargan, K., N. Kramarova, B. Weir, S. Pawson, and S. Davis (2020). Towards a reanalysis of stratospheric ozone for trend studies: Assimilation of the Aura Microwave Limb Sounder and Ozone Mapping and Profiler Suite Limb Profiler data. *J. Geophys. Res. - Atmos.*, 125, e2019JD031892. doi: 10.1029/2019JD031892.

Waugh, D. W., & Eyring, V. (2008). Quantitative performance metrics for stratospheric-resolving chemistry-climate models. *Atmospheric Chemistry and Physics*, 8, 5699–5713. https://doi.org/10.5194/acp-8-5699-2008

Wesely, M. L. (1989). Parameterization of Surface Resistances to Gaseous Dry Deposition in Regional-Scale Numerical-Models, *Atmos. Environ.*, 23, 1293-1304, http://doi/.org/Doi 10.1016/0004-6981(89)90153-4.

Wilczak, J., S.A. McKeen, I. Djalalova, et al. (2006). Bias-corrected ensemble and probabilistic forecasts of surface ozone over eastern North America during the summer of 2004, *J. Geophys. Res.*, 111 (D23S28), 10.1029/2006JD007598

Winer, A. M., J. W. Peters, J. P. Smith, and J. N. Pitts Jr. (1974), Response of commercial chemiluminescence NO–NO2 analyzers to other nitrogen-containing compounds, *Environ. Sci. Technol.*, 8, 1118–1121.

Wu, W.-S., R.J. Purser and D.F. Parrish (2002). Three-dimensional variational analysis with spatially inhomogeneous covariances. *Mon. Wea. Rev.*, 130, 2905-2916.

Zhang, Y., Jacob, D. J., Lu, X., Maasakkers, J. D., Scarpelli, T. R., Sheng, J.-X., Shen, L., Qu, Z., Sulprizio, M. P., Chang, J., Bloom, A. A., Ma, S., Worden, J., Parker, R. J., and Boesch, H. (2020), Attribution of the accelerating increase in atmospheric methane during 2010–2018 by inverse analysis of GOSAT observations, *Atmos. Chem. Phys. Discuss.*, https://doi.org/10.5194/acp-2020-964, in review.